Performance of Precast Industrial Buildings During the 1999 Earthquakes in Turkey

by

Mauricio Posada, B.S.

Thesis

Presented to the Faculty of the Graduate School of

The University of Texas at Austin

in Partial Fulfillment

of the Requirements

for the Degree of

Master of Science in Engineering

The University of Texas at Austin

December 2001

Performance of Precast Industrial Buildings During the 1999 Earthquakes in Turkey

Approved by
Supervising Committee:

Sharon Wood, Supervisor

Michael Kreger

Dedication

To my beautiful family and Joojita

Acknowledgements

The work described in this thesis was performed in conjunction with a cooperative research program sponsored by the U.S. National Science Foundation to investigate the performance of precast buildings during the 1999 earthquakes in Turkey. The opinions expressed in this thesis are not necessarily those of the sponsor.

I would like to especially thank Professor Sharon Wood for her support, guidance and patience, which were exceptional and vital for the accomplishment of this work. As advisor, professor, and person I will always remember her for all the help and advice she gave me during my Master.

I also appreciate the great opportunity of visiting Turkey as part of the research work, in particular I would like to thank Professors Sharon Wood, Michael E. Kreger and Eric B. Williamson who gave me this nice opportunity.

The assistance of faculty at the Middle East Technical University (METU) and engineers from the Turkish Precast Association, TPCA are gratefully acknowledged.

In general, I would like to thank The University of Texas. I came full of illusions and dreams and now everything has been accomplished due to all the support that I have received. I will always have U.T. in my mind and heart.

I would finally like to thank my the friends, I wish for them the best future; my parents and sister who are the most important part of my life and feel this success also as theirs; and Mina, my dear love, who gave me not only

distraction but also inspiration in the final part of the Master; with all of them I share this huge happiness.

December 5, 2001

Abstract

Performance of Precast Industrial Buildings During the 1999 Earthquakes in Turkey

Mauricio Posada, M.S.E.

The University of Texas at Austin, 2001

Supervisor: Sharon Wood

Precast frame buildings are frequently used in Turkey for industrial facilities. One-story warehouses are the most common structural configuration. Many precast buildings collapsed during the 1999 earthquakes in Turkey (Kocaeli and Düzce earthquakes). In the present investigation, a parametric approach is developed to study the relationship between structural stiffness and the observed damage to one-story precast warehouses in the epicentral region.

Table of Contents

List of Tables

List of Figures

CHAPTER 1
Introduction

1.1 DESCRIPTION OF THE EARTHQUAKES OF AUGUST 17 AND NOVEMBER 12, 1999

On August 17 and November 12, 1999, large earthquakes shook the Anatolian region in northwest Turkey (see Figure 1.1). The former was named the Kocaeli earthquake ("Marmara earthquake" in some publications), and the latter was named the Düzce earthquake. Aschheim (2000) commented that the Turkish National Security Council estimated that 115,000 buildings were damaged beyond repair and more than 500,000 people were left homeless by the two earthquakes. Lettis (2000) indicated that the tectonic framework associated with the 1999 earthquakes is related to the collision of the following three plates: the Arabian, the African and the Eurasian, as can be seen in Figure 1.2. The zone is crossed by the North Anatolian fault, a strike-strip fault.

The epicenter of the Kocaeli earthquake was east of Gölcük (Atakoy, 1999) and the epicenter of the Düzce earthquake was south of Düzce. Figure 1.3 illustrates the locations of the epicenters, and the 126-km and 39-km rupture lengths from the Kocaeli and Düzce earthquakes, respectively. In addition, the magnitudes (M_w = 7.4 and M_w = 7.1) and some of the vertical offsets are also shown in Figure 1.3.

Geotechnical damage such as ground failure and liquefaction of soils was widely observed. These effects intensified the structural damage of many buildings.

Figure 1.1 Map of Turkey - Region Affected by the 1999 Earthquakes

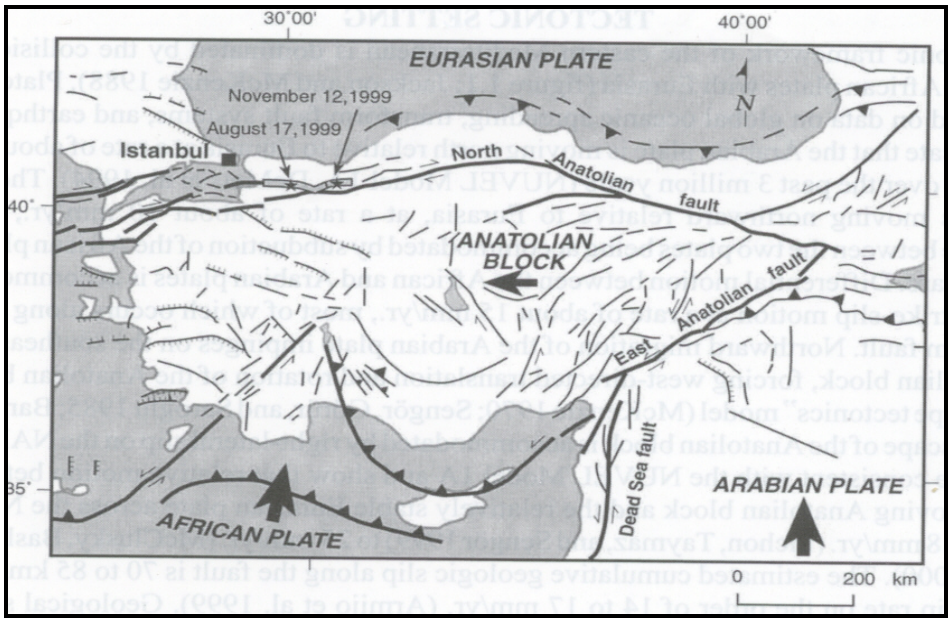

Figure 1.2 Tectonic Framework of the Anatolian Region

(Taken from Lettis, 2000)

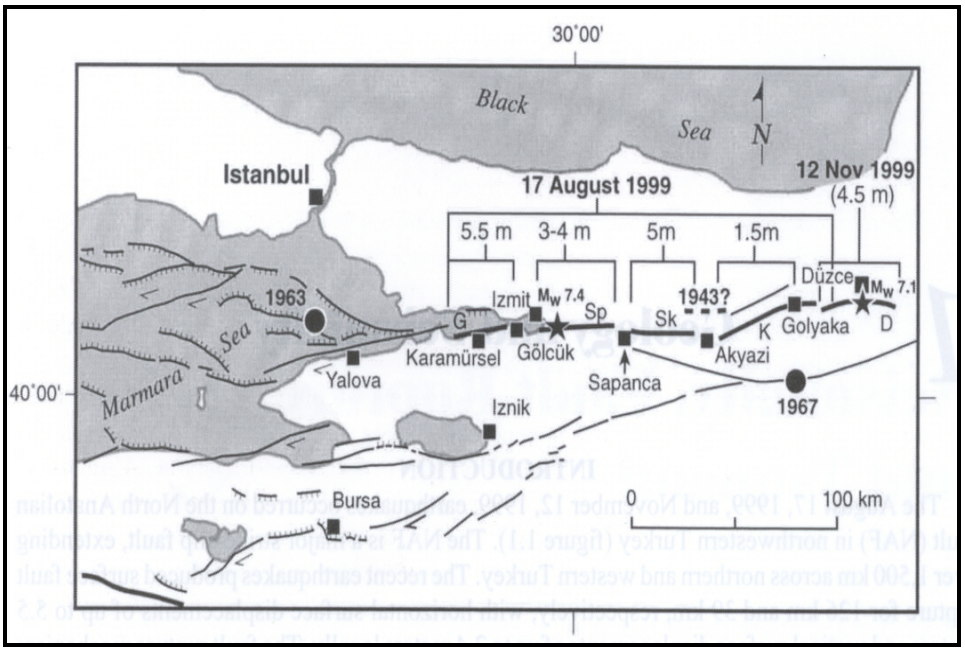

Figure 1.3 Kocaeli and Düzce Earthquake Epicenters, Rupture Lengths, and Surface Offsets (Taken from Lettis, 2000)

1.2 GENERAL DESCRIPTION OF THE EPICENTRAL REGION BUILDINGS

The epicentral region is a highly industrialized zone. Almost 20 million people (one third of the Turkish population) live in this region, which includes Istanbul (Scawthorn, 2000). Forty years ago, 65% of the population of Turkey lived in rural areas; however, this figure has fallen to 40% today. In the last 20 years, the epicentral region has experienced very rapid growth due to industrialization. Johnson (2000) indicated that the epicenter region is home to about 40% of Turkey's heavy industry. Large petrochemical complexes, manufacturing plants, automotive industry, and civil and military ports are also located in this region.

The housing and commercial demand due to this high growth rate has been met, in general, by reinforced concrete buildings with masonry infill (Aschheim, 2000). Three to seven-story buildings based on reinforced concrete beam-column frames with hollow clay partitions are the most common residential structures in the epicenter region. In many cases, the construction was completed using an incremental system (Aschheim, 2000) in which inhabitants added new stories over time. Column reinforcing bars protrude above the current roof slab to facilitate the construction of additional stories in the future when the inhabitants can afford to increase the height of the building.

The industrial plants in the epicentral area are usually built with structural steel or precast concrete. For relatively long spans, steel truss-frame systems with bolted connections are frequently used. Bolted connections (Aschheim, 2000) provide some moment resistance for lateral loads; however, during the earthquakes, some of these connections failed. In addition, the use of precast concrete buildings for industrial plants has become popular because of the relatively low construction cost and the ability to create large open areas for manufacturing. Some precast concrete buildings have been designed and built with moment resisting connections, but in general, pinned connections at the roof level have been used. Precast buildings in the epicentral region are typically one to three-stories; however, the single-story structures represent the most common form of precast construction and a large portion of the structures that sustained damage during the 1999 earthquakes. For this reason, the present study will focus on the one-story precast industrial buildings (see Chapter 2).

Chapter 2 describes the precast concrete buildings and explains the structural systems in more detail. A description of the structural damage observed in this type of buildings is also presented in Chapter 2. The ground motion records and elastic response spectra used in the investigation are described in Chapter 3.

Chapters 4, 5 and 6 study three potential types of structural damage in the one-story buildings: the transverse drift capacity, the impact damage at the connection between the column and the roof girders, and the out-of-plane movement of roof girders. Finally, conclusions of the investigation are presented in Chapter 7. Acceleration histories, response spectra, and moment – curvature plots are included in the Appendices.

CHAPTER 2
Description of the Precast Concrete Buildings

2.1 INTRODUCTION

Precast concrete construction has been widely used throughout Turkey for variety of purposes, and it is often used for industrial facilities. Chapter 2 provides a briefly description of precast multi-story systems, and then discusses one-story buildings, which are the most widely used and the type of structure that sustained the most damage during the 1999 earthquakes. In addition, a description of the Turkish Precast Association is presented in this chapter. Finally, the types of structural damage observed in the one-story buildings are described.

2.2 MULTI – STORY BUILDINGS

Some precast concrete multi-story buildings are present in the epicentral region, especially around İstanbul, for office and industrial purposes. These buildings (Figures 2.1 and 2.2) are usually rectangular in plan, with precast girders, purlins, and gutter beams for the roof system. Pinned connections are common joining purlins and roof girders.

Precast columns with corbels typically support hollow-core planks as shown in Figure 2.1. The foundation system used consists of socket footings and grade beams (Figure 2.1). The beam-column connections are moment - resisting, except to the roof-girder connections, which are pinned. Figure 2.2 shows a multi-story industrial building in the epicentral region.

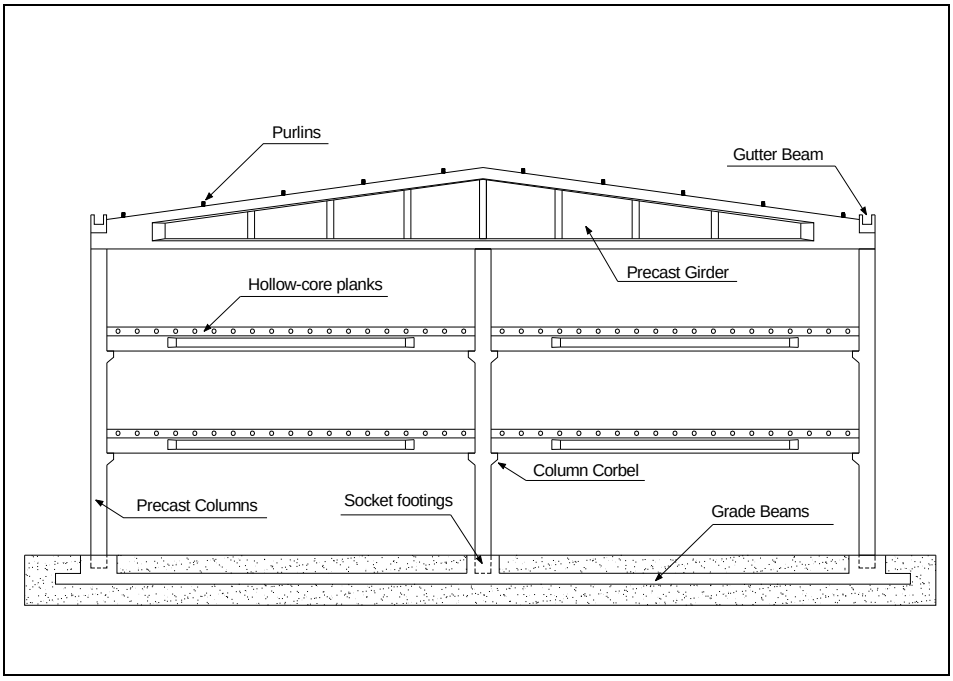

Figure 2.1 Transverse Elevation of a Typical Multi-Story Precast Building

Figure 2.2 Interior Photograph of a Multi-story Precast Building

A thin topping slab is cast over the hollow-core planks. These planks, shown in Figure 2.3, are produced in precast plants.

Figure 2.3 Hollow-core Planks Used for Intermediate Floors in Multi-story Buildings

2.3 ONE – STORY BUILDINGS

The one-story industrial buildings observed in the epicentral area are, in general, rectangular in plan with one to four bays in the transverse direction and ten to thirty bays in the longitudinal direction (Figure 2.4). Usually, the length of the transverse bays ranges from 10 to 25 m, and the length of the bays in the

longitudinal direction range from 6 to 8 m. Story heights typically range from 6 to 8 m.

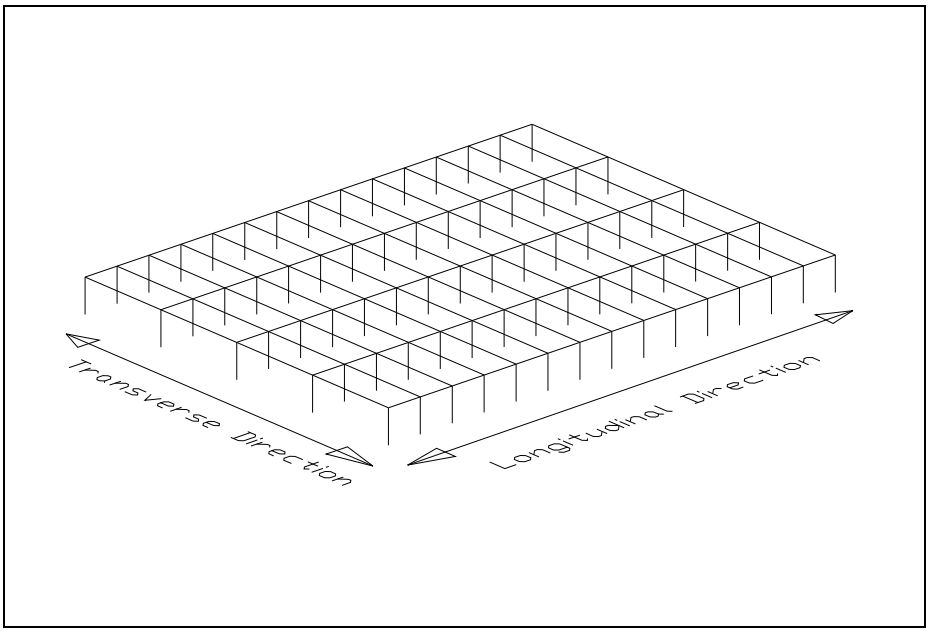

Figure 2.4 Typical Geometry of the One-story Precast Concrete Building

The structural system for the one-story industrial buildings is based on rectangular precast columns fixed at the base, and long-span roof girders that are oriented along the transverse axis of the building. The shape of these roof girders is typically triangular (Figure 2.5). In addition, working as gutter beams to collect the water from the roof, beams with U-shaped cross section span in the longitudinal direction. Purlins for the roof system, oriented in the longitudinal direction, are present as well. The roof is constructed using lightweight materials, such as metal decking or asbestos panels.

Although there are some one-story industrial buildings with moment-resisting connections, the general case is pinned connections (deformed dowels)

at the ends of the beams, girders and purlins. Clay tile infill and precast concrete panels are also used as exterior walls and division partitions. However, these walls do not contribute to the lateral stiffness of the building. The lateral strength and stiffness are provided only by the cantilevered columns.

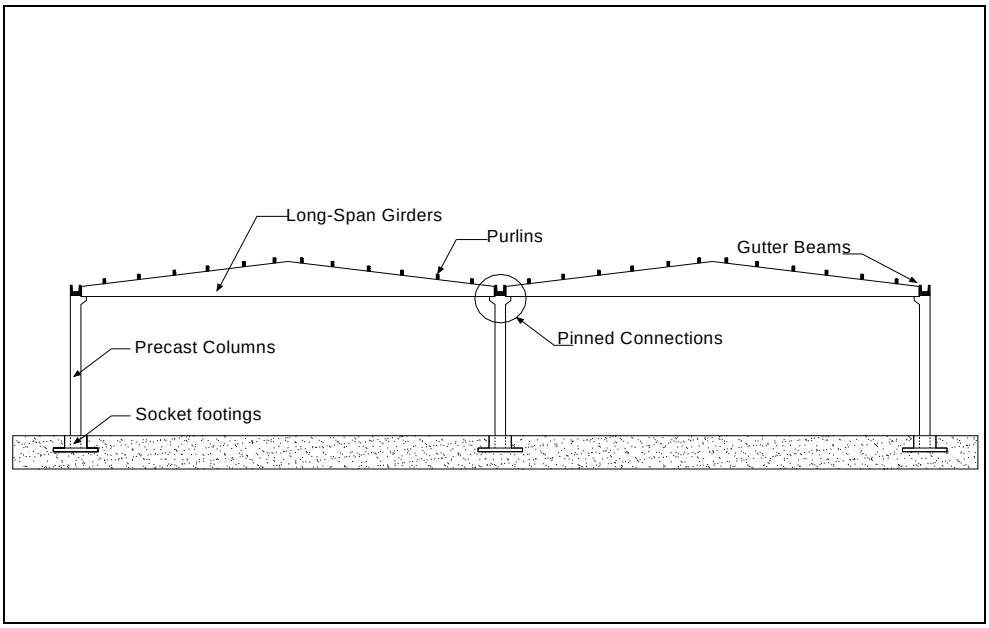

Figure 2.5 Elevation of a Typical One-story Precast Concrete Building

2.4 THE TURKISH PRECAST ASSOCIATION

In 1984, the Turkish Precast Association (TPCA) was established to promote the use of precast concrete in the country, to develop standards and specifications for the industry, and to improve the use of precast construction (TPCA, 2000). The TPCA operates 40 facilities and has an annual production capacity of 2.5 million tons (50% of Turkish precast construction) (Karaesmen, 2001). However, only 30% of the precast companies in Turkey are affiliated with

the association. The TPCA produces precast elements for offices, houses, and hospitals, and also for commercial and industrial buildings.

The TPCA surveyed 481 buildings that had been constructed by TPCA members after the Kocaeli earthquake (Atakoy, 1999), and less than 10% sustained damage; however, the percentage of damaged buildings built by non-TPCA members was larger. Atakoy (1999) identified two main problems with the damaged buildings: underestimation of the soil properties, leading to the use of lower spectral acceleration in the design, and inadequate lateral stiffness. This second cause of damage was investigated in more depth in this investigation.

2.5 TYPES OF STRUCTURAL DAMAGE OBSERVED IN THE ONE-STORY INDUSTRIAL BUILDINGS

Some of the structural damage observed in the one-story industrial buildings consisted of flexural hinges at the base of the columns, longitudinal movement of the roof girders (producing unseating and then total collapse), and out-of-plane movement of roof girders, producing rotation or tilting of the supports.

Figures 2.6 and 2.7 show photographs of plastic hinges that formed at the base of the columns, with an approximate length of 1 m. Figure 2.6 shows the cracks produced along the plastic length (up to 10 mm wide). Figure 2.7 shows a severe case where the plastic mechanism created, generated the total collapse of the column. The footings did not show any signs of distress, as illustrated in Figure 2.7.

Figure 2.8 shows large drift ratios observed in the industrial buildings. It can also be seen, that large levels of distortion led to unseating of roof girders, and therefore collapse of the roof. In general, this behavior could be considered

Figure 2.6 Plastic Hinge at the Base of Columns in a One-story Building near Adapazari

Figure 2.7 Plastic Hinge at the Base of Columns in a One-story Building near Gölcük

as the main factor of collapse of the structures studied; therefore it will be studied in more detail in Chapter 4 where a parametric study is carried out using different column sizes and reinforcement ratios for some of the ground motions recorded in the 1999 earthquakes.

Figure 2.8 Large Drift Ratios Observed in Precast Buildings near Adapazari

Several problems were identified with the column-girder connections. In this frame system, the girders are very stiff and the columns are flexible. When the structure is excited by an earthquake, the column rotates and the girder, due to its stiffness, tends to remain horizontal. Figure 2.9 illustrates the spalling that results due to the impact between the girder and the gutter beam and column. The impact could

cause spalling of the concrete from the roof girder, column or gutter beam. Figure 2.9 illustrates the case where the concrete spalled off the end of the roof girder due to the impact, and thus some of the reinforcement is exposed. Chapter 5 explains this situation in detail.

Figure 2.9 Concrete Spalling due to Impact when the Column Rotates

Many of the buildings were under construction during the 1999 earthquakes; therefore connection details (Fig. 2.10), such as the grout around the column dowels were not finished completely at the time of the shaking. Figure 2.11 shows a column-girder connection where the lack of bolts at the top of the dowel (above the girder) and lack of grout (filling the dowel holes) permitted the relative displacement of the members. In some cases out-of-plane tilting was

observed, this situation was also associated with the fact that the construction was not fully complete.

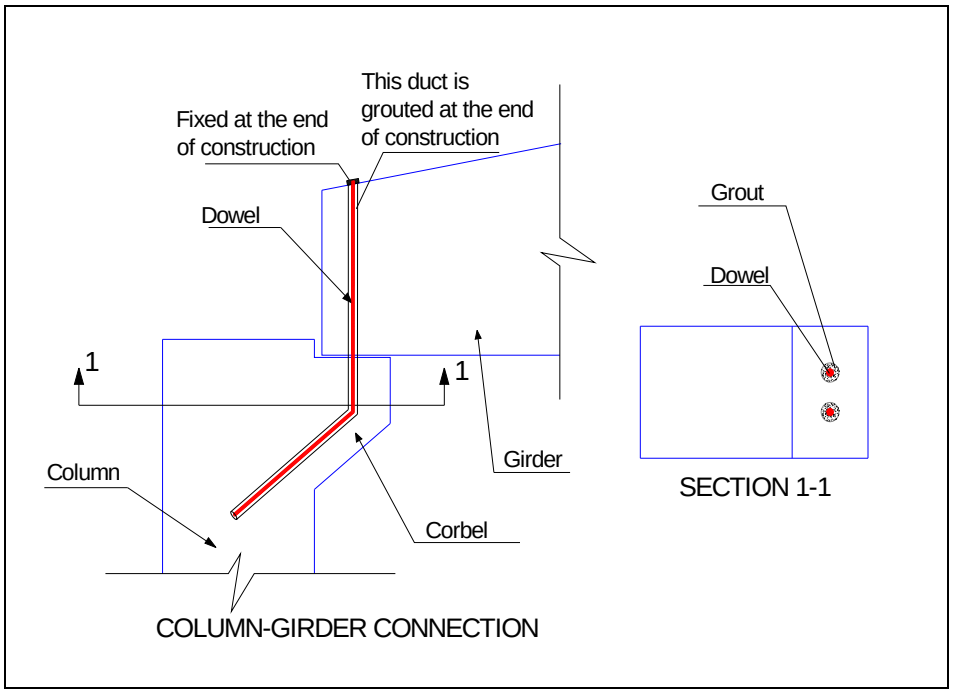

Figure 2.10 Column-Girder Connections – Grouted Dowel

In general, precast buildings sustained significant damage during the 1999 earthquakes in Turkey. Figure 2.12 illustrates the case of a complete building collapse. Evidence of all three potential collapse mechanisms was observed in this building. However, in some cases no damage was observed, such as the building shown in Figure 2.13.

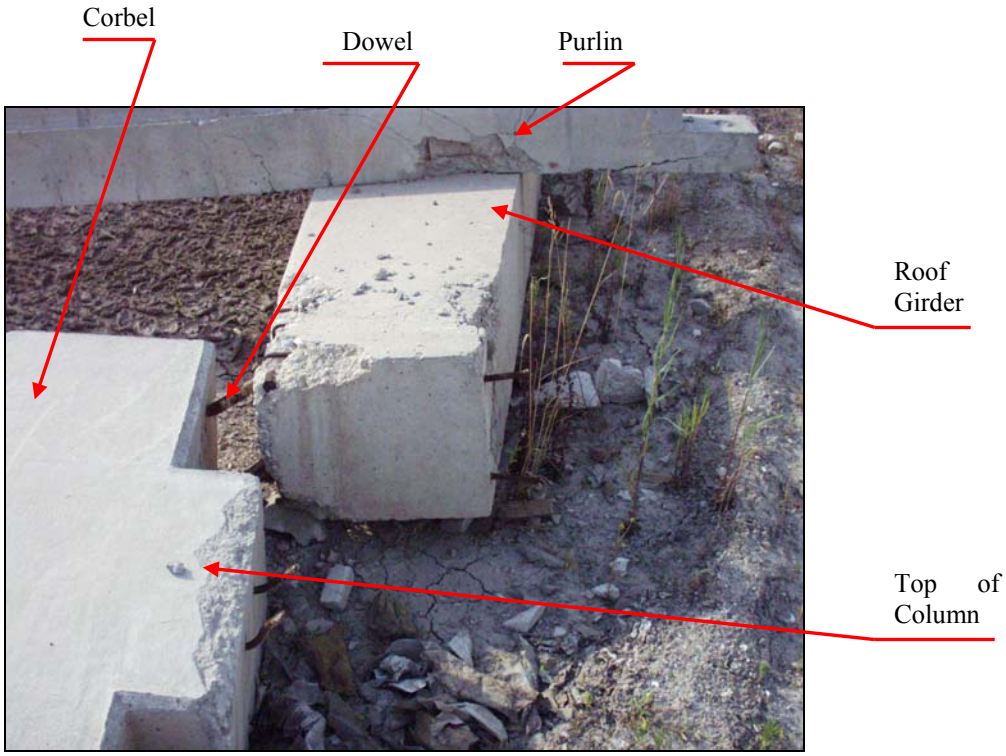

Figure 2.11 Column-Girder Connections Problems

Figure 2.12 General Collapse of a Precast Building near Gölcük

Figure 2.13 Building with no damage near Düzce

CHAPTER 3
Ground Motions

3.1 ACCELEROGRAMS

A large number of ground motions were recorded in northwest Turkey during the 1999 earthquakes. For the purposes of the study, eleven ground motion records from the Kocaeli earthquake and four from the Düzce earthquake were used. As can be seen in Table 3.1, these records correspond to eight stations, most of which are within 50 km of the epicenters of the earthquakes, and all are within 20 km of the fault trace (Rathje, 2000).

The Gebze, Arcelik and Sakarya records were measured on stiff soil, İzmit on rock, and the others were recorded on soft alluvial soil deposits (see Table 3.1). All the records, except Sakarya, were recorded normal and parallel to the fault (the north-south component of the Sakarya station did not function during the earthquake). The peak horizontal accelerations are plotted as a function of the epicentral distance in Figure 3.1. The peak acceleration was less than 0.5g for most of the records, but exceeded 0.7g for both components of ground motion recorded in Bolu.

Anderson (2000) explained the possible causes of the large peak accelerations recorded in Bolu during the Düzce earthquake. Although the recording station in Bolu was 42 km from the epicenter of the Düzce earthquake, the peak accelerations (0.74g and 0.81g) were significantly larger than the peak accelerations recorded in Düzce (0.41g and 0.51g). Site response caused by sediment amplification and the directivity-focusing phenomenon may have contributed to the large peak accelerations in Bolu.

The accelerograms from the 15 ground motion records are presented in the Appendix A. The duration of the records motion varies from 25 to 75 seconds, except Sakarya, where 150 seconds of motion were recorded. In most of the records the arrival times of the P-waves and the S-waves are obvious.

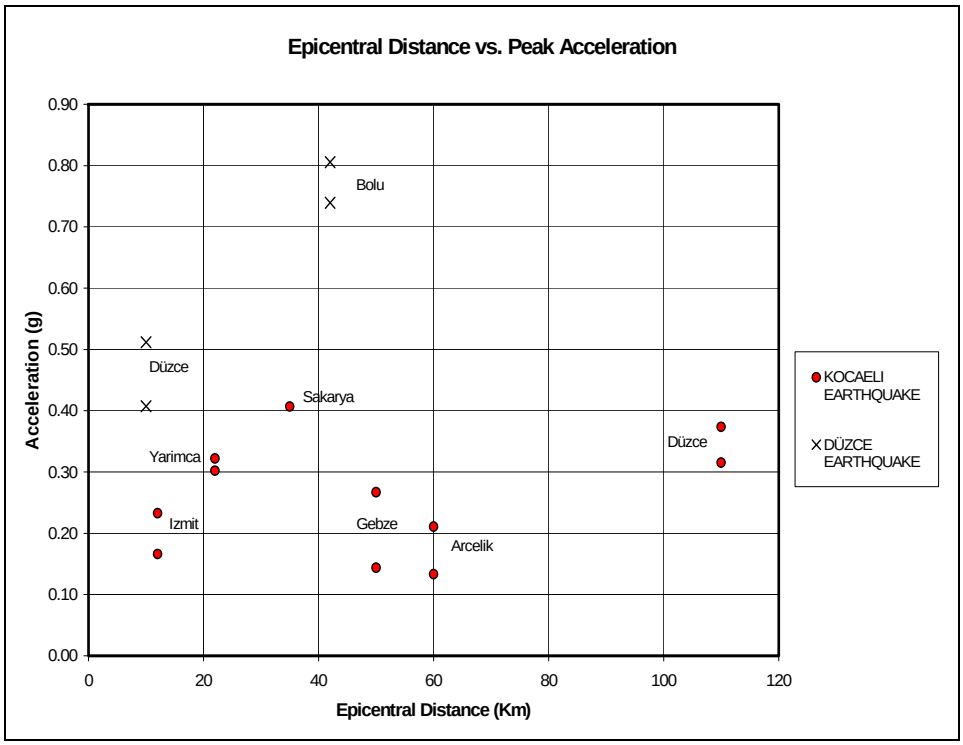

Figure 3.1 Ground Motion Records Used in the Study

Table 3.1 Ground Motions Considered in the Study

Earthquake	Station	Comp.	Peak Acc (g)	Epicentral Distance (km)	Distance to fault rupture plane (km)	Soil Conds.
Kocaeli	Arcelik (ARC)	000	0.21	60	17	Stiff Soil
		090	0.13			
	Düzce (DZC)	180	0.32	110	14.2	Soft Soil
		270	0.37			
	Gebze (GBZ)	000	0.27	50	17	Stiff Soil
		270	0.14			
	İzmit (IZT)	090	0.23	12	7.7	Rock
		180	0.17			
	Sakarya (SKR)	090	0.41	35	3.3	Stiff Soil
	Yarimca (YPT)	330	0.32	22	4.4	Soft Soil
		348	0.30			
Düzce	Bolu (BOL)	000	0.74	42	19.9	Soft Soil
		090	0.81			
	Düzce (DZC)	180	0.41	10	8.3	Soft Soil
		270	0.51			

3.2 SPECTRA

For the 15 ground motion records described above, elastic acceleration, velocity and displacement response spectra were computed for a 2% damping ratio. The computer program *RespSpect2000 ver1.2*® developed by Professor Luis

E. Garcia was used to produce the elastic spectra. The spectra for the 15 ground records are presented in the Appendix B.

Maximum, minimum and average acceleration spectra for soft soil and stiff soil/rock are plotted in Figures 3.2 and 3.3, respectively. For periods less than 0.20 seconds the spectral accelerations for both types of soil are very similar. However, for longer periods the difference is considerable; the maximum spectral accelerations for the stiff soil sites are similar to the minimum spectral accelerations for the soft soil sites.

The maximum, minimum, and average spectral displacements are plotted for soft and stiff soil/rock, in Figures 3.4 and 3.5 respectively. In general the mean spectral displacement for the soft soil sites is two times larger than the mean spectral displacement for the stiff soil/rock sites.

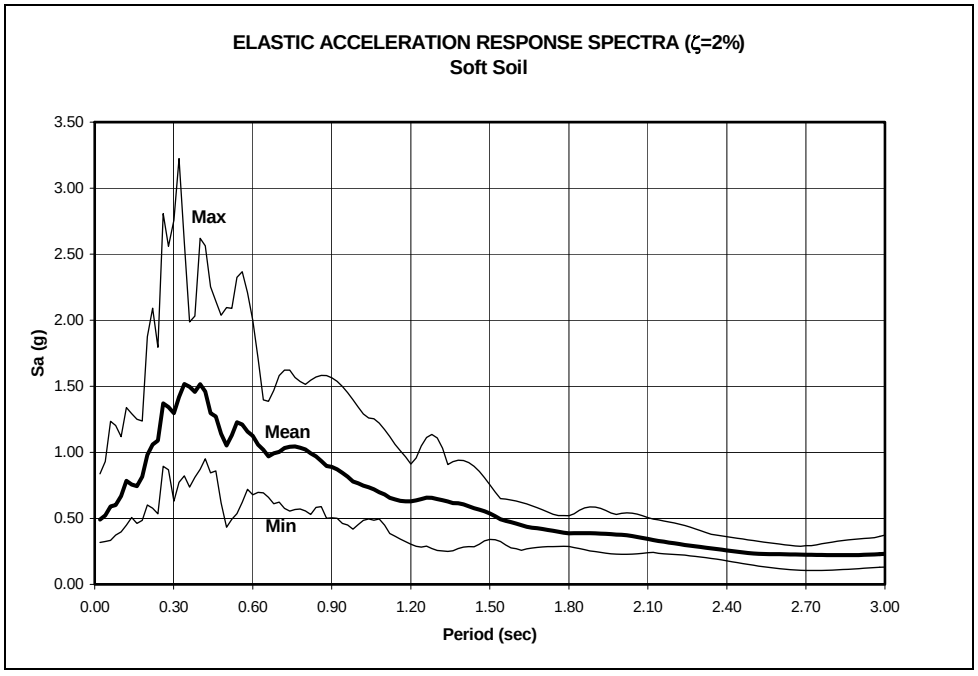

Figure 3.2 Acceleration Response Spectra for Soft Soil Sites

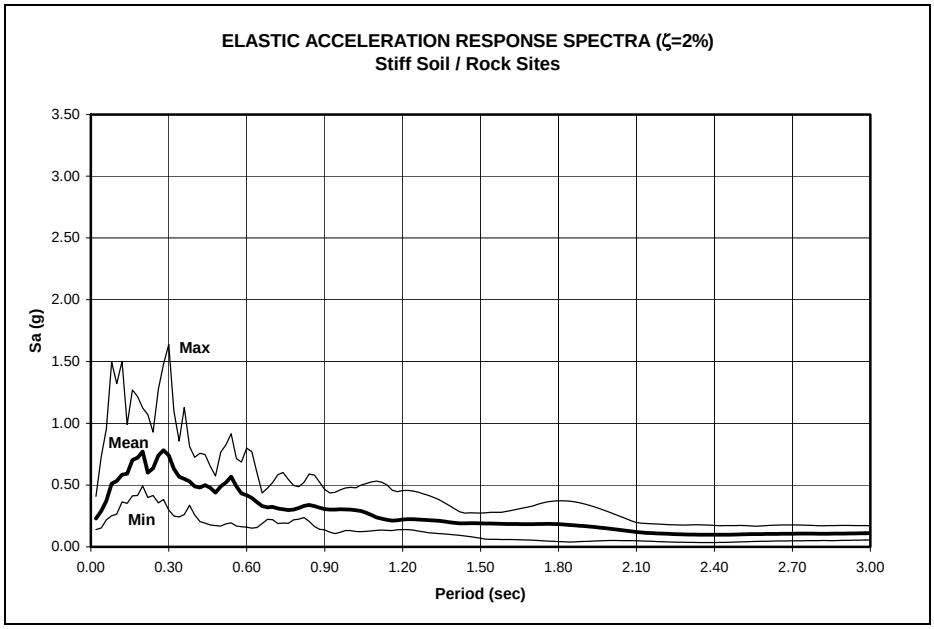

Figure 3.3 Acceleration Response Spectra for Stiff Soil and Rock Sites

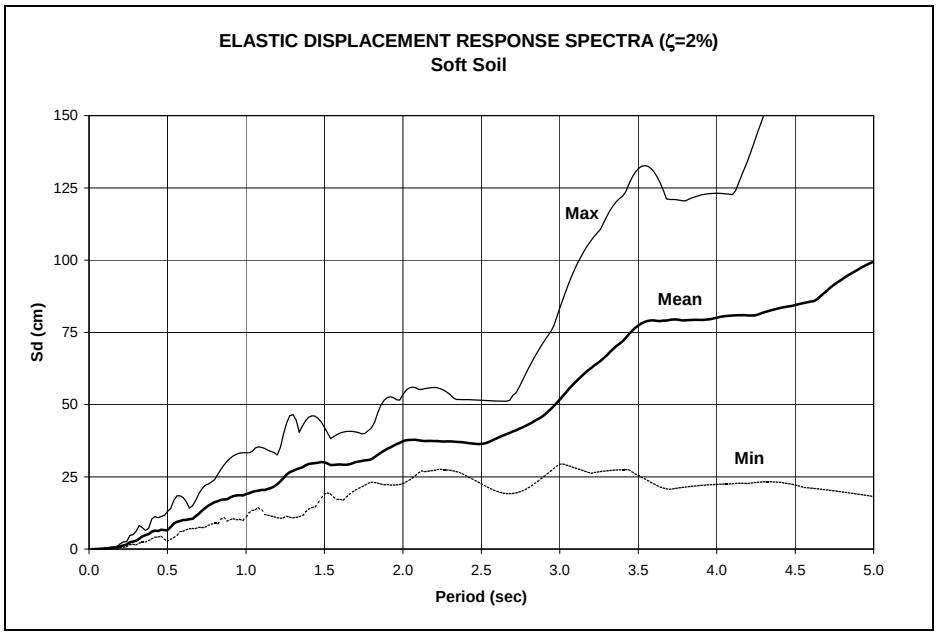

Figure 3.4 Displacement Response Spectra for Soft Soil Sites

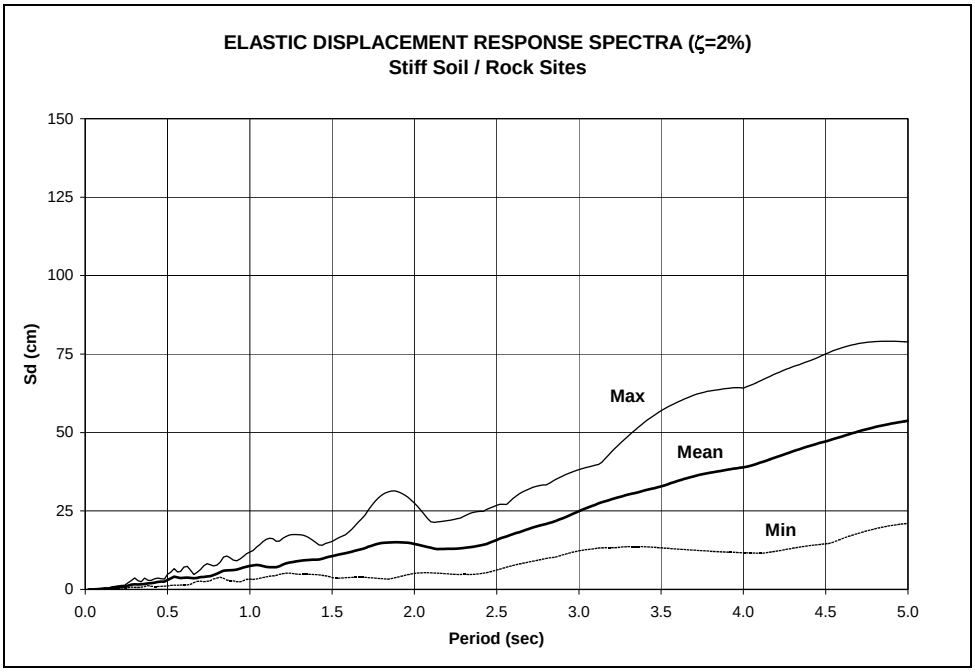

Figure 3.5 Displacement Response Spectra for Stiff Soil and Rock Sites

CHAPTER 4
Drift Capacity

4.1 OBJECTIVE

As was mentioned in Chapter 2, one of the most common collapse mechanisms observed in the epicentral region was caused by large drift ratios in the transverse direction of the buildings. The large lateral distortions caused unseating of the roof girders and collapse of the roofs, as shown in Figure 4.1.

Figure 4.1 Large Transverse Drift Ratios

A parametric approach was developed to study the relationship between the lateral stiffness of the structures and the calculated drift ratios. The parametric study focused on the behavior of the columns, due to their importance as the main structural elements for lateral strength and stiffness, and also because plastic hinges were observed at the base of many columns. The primary parameter studied was the column size, i.e. the cross-sectional dimensions of the columns. Seventeen different sizes were considered from 40x40 cm up to 100x100 cm. First, a single computer model was created. Fifteen ground motions recorded during the 1999 earthquakes were used as input. For each column size, the elastic displacement at the roof level was calculated. The results indicated a wide range of drift ratios for all the column sizes and ground motion records. In order to compare earthquake demand with column capacity, moment-curvature analyses were developed for three different longitudinal reinforcement ratios. Using the results of the moment-curvature analyses and the moment-area theorems, drift ratios corresponding to yielding of the reinforcement and capacity were computed for each column size. Finally, the drift ratios due to the earthquake demand were compared with the displacement capacities of the columns to determinate required levels of stiffness.

4.2 PROTOTYPE BUILDING

As described in Chapter 3, eleven ground motion records from the Kocaeli earthquake and four from the Düzce earthquake were used in the parametric study.

A one-story precast building was modeled following a prototype chosen by the project team. The building corresponds to a plant close to Adapazari (Figure 4.2). The structural drawings were provided by the precast producer to the

project team. Figure 4.3 shows the prototype floor plan. The building comprises 26 longitudinal bays, each 7.50 m wide and 4 transverse bays, each 20 m wide. The building height is 7m. The building follows the typical geometry and bay sizes described in Chapter 2. The framing system in the transverse direction was modeled using the 2-D model shown in Figure 4.4. The connections between columns and girders were modeled as pinned. The mass of the girders, beams, purlins, roofing materials, cladding, and half of the columns were lumped at the upper joints.

Figure 4.2 Prototype Building

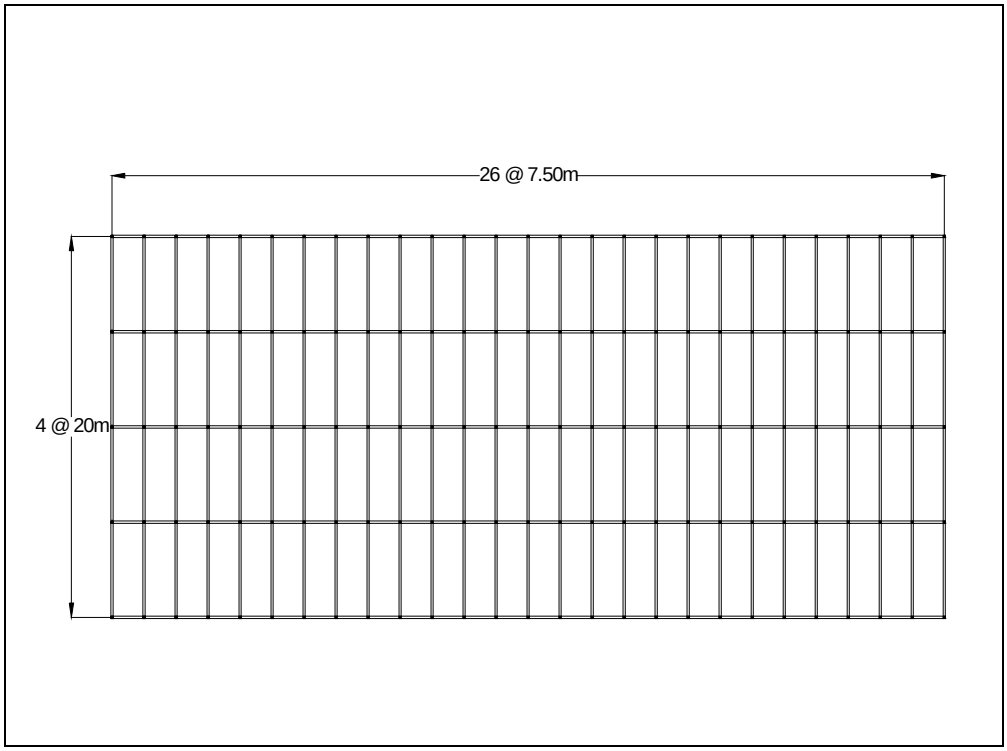

Figure 4.3 Prototype Floor Plan

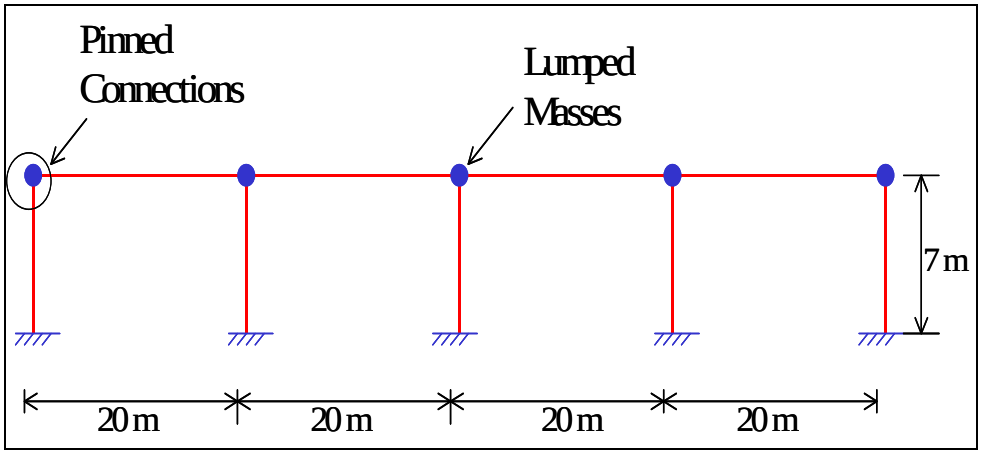

Figure 4.4 2D Linear Model of the Framing System in the Transverse Direction

4.3 ANALYTICAL MODEL

The linear-elastic model was created using the finite element program SAP2000. Frame elements were used for the girders and columns of the four-bay structure. Figure 4.5 shows the model. The base of each column was restrained against rotation and displacement. The connections between the column and girder elements were modeled as pins using frame releases for the bending moment. Figure 4.6 shows the deformed shape and the bending moments due to an elastic response spectrum input. It can be seen that the effect of the releases introduced in the upper joints produces zero moment in the girder- column connection; that is precisely the situation desired. For the girders, the non-prismatic section option was used, and the girder was divided into four sections, using the cross-sectional dimensions at the ends, center and quarter points of the 20-m span. The cross sections of the tapered girder are shown in Figure 4.7. These particular dimensions correspond to the prototype building described in Section 4.2.

The masses of the purlins and roof were computed and are lumped in the upper joints (Figure 4.5). The arrows indicate the degrees of freedom to which the masses were assigned.

The roof and purlin masses were computed in the following way, assuming 7.5 m bay spacing in the longitudinal direction and ten purlins per transverse bay:

For the interior joints:

$$Roof : (200N/m^2) : 200N/m^2 \times 20m \times 7.5m = 30000N = 3000Kg(mass)$$

$$Purlins : (10units) : 0.0226m^2 \times 7.5m \times 24000N/m^3 \times 10units = 40680N$$

= 4068 Kg (mass)

Total mass for interior joints: *7068 Kg (mass)*

For the exterior joints:

$$Roof : (200N/m^2) : 200N/m^2 \times 10m \times 7.5m = 15000N = 1500Kg(mass)$$

$$Purlins : (5units) : 0.0226m^2 \times 7.5m \times 24000N/m^3 \times 5units = 20340N$$

= 2034 Kg (mass)

Total mass for exterior joints: *3534 Kg (mass)*

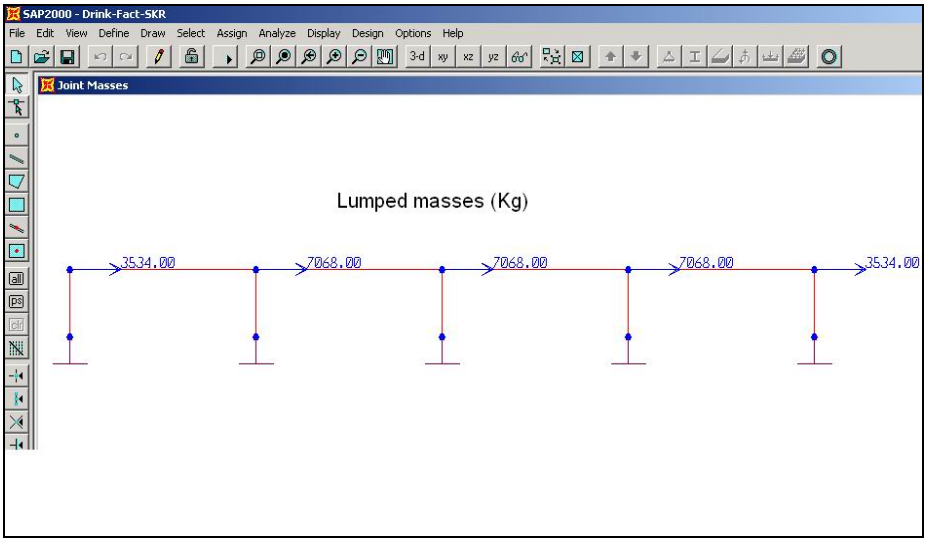

Figure 4.5 SAP2000 Linear–Elastic Model (Lumped Masses Displayed)

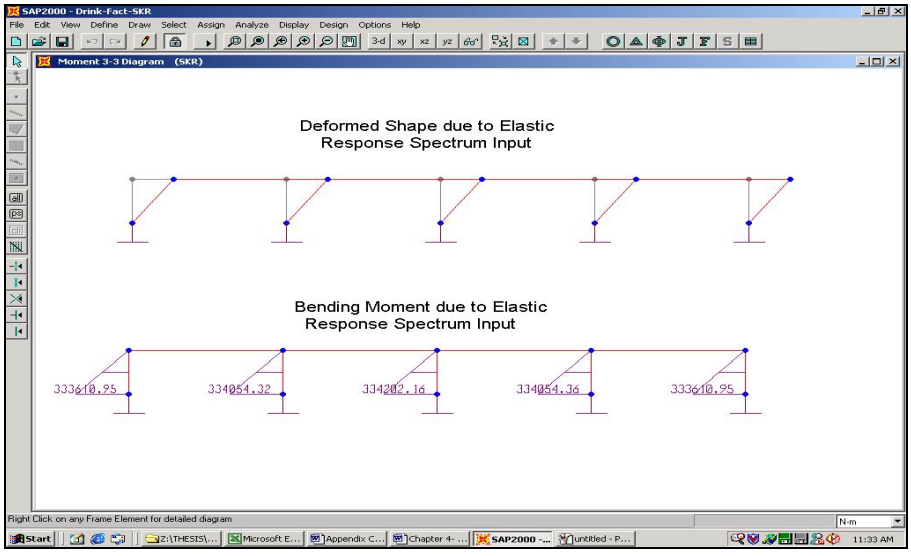

Figure 4.6 SAP2000 Linear-Elastic Model (Deformed Shape and Bending Moments Displayed)

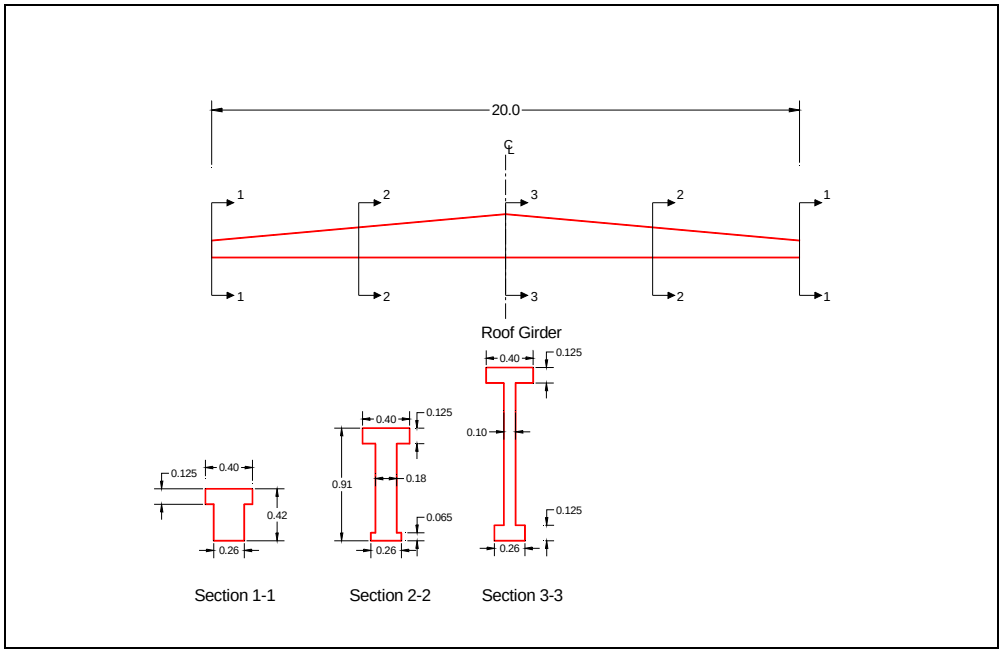

Figure 4.7 Roof Girder, Cross sections

The primary parameter studied in this series of analyses was the cross-sectional dimensions of the columns. Seventeen different sizes were considered from 40x40 cm up to 100x100 cm; 40x40 was the smallest size observed in the field. The largest size observed was 80x80 cm in the Ford Plant near Gölcük. The 2D model described above was analyzed with each column size. The calculated natural period for each system is listed in Table 4.1. In addition, it is possible to estimate the natural period corresponding to cracked cross-sectional properties. Shimazaki and Sozen (1984) indicated that the period for a cracked section could be approximated as:

$$T_e = T_i \cdot \sqrt{2} \qquad \textbf{Equation 4.1}$$

Where T_i is the initial period calculated using gross cross-sectional properties, and T_e is the effective period of the structure.

The relationship between the column dimension and the natural period is expected because the larger the cross-sectional area, the larger the moment of

inertia, the larger the natural frequency (ω), and the smaller the natural period ($T=2\pi/\omega$). Figure 4.8 shows the direction of the motion analyzed and the definition of b and h, in order to interpret the data summarized in Table 4.1

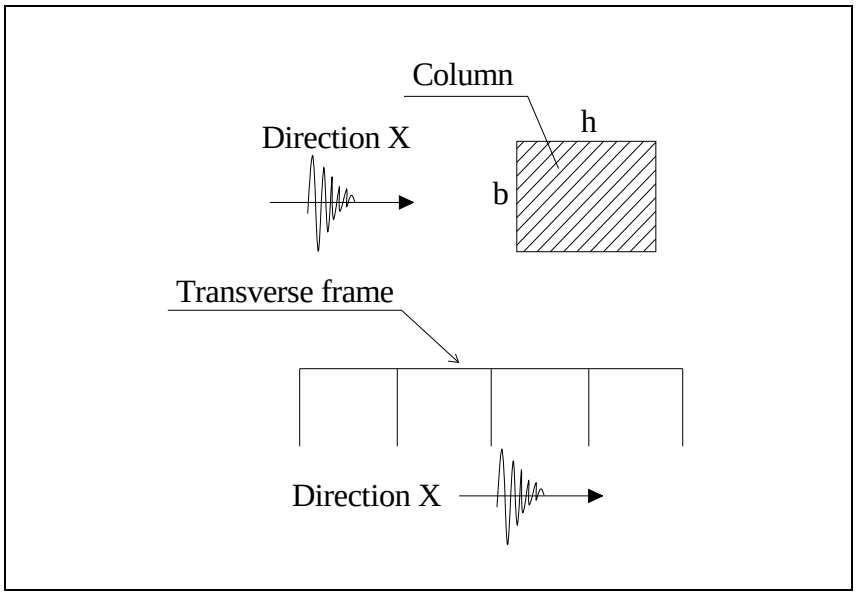

Figure 4.8 Motion Direction, b and h Definition

Table 4.1 Column Sizes Used for the Parametric Study and Calculated Periods

Column Dimensions		**Period, T_i * (sec)**	**Period, T_e ** (sec)**
b (cm)	**h (cm)**		
40	40	1.10	1.56
45	40	1.05	1.48
40	45	0.93	1.32
45	45	0.88	1.25
40	50	0.80	1.13
45	50	0.76	1.07
50	50	0.73	1.03
55	50	0.70	0.99
50	55	0.64	0.90
55	55	0.61	0.86
55	60	0.54	0.76
60	60	0.52	0.74
65	65	0.45	0.64
70	70	0.40	0.56
80	80	0.31	0.45
90	90	0.26	0.37
100	100	0.22	0.31

* Period calculated using gross cross-sectional properties for columns.

** Period calculated using cracked cross-sectional properties for columns.

4.4 CALCULATED EARTHQUAKE DEMAND

The next step in the study is the computation of the drift demand in the idealized structure. Each of the models is run for each of the column sizes and each of the ground motion records; therefore, 255 points can be plotted (17 column sizes and 15 ground motion records). As described in Chapter 3, elastic acceleration response spectra for 2% damping ratio were developed for each of the ground motion records. These spectra are the input for the modal analysis developed with SAP2000. In each run, the maximum roof displacement is recorded, and then, in order to obtain the drift ratio, the roof displacement is divided by the column height (7 m). The damping ratio used for the analyses is 2%, because the elastic demand will provide an upper bound to the inelastic demand (Shimazaki and Sozen, 1984).

Table 4.2 shows the drift ratios for each of the ground motion records and each of the column sizes studied (as a function of the calculated natural period corresponding to cracked cross-sectional properties). In order to evaluate the results, it is more convenient to separate the earthquake demand in two groups according to the ground motion record (soft soil and stiff soil/rock), as discussed in Chapter 3 (Figures 4.9 and 4.10). Figure 4.9 shows the earthquake demand for soft soil. It can be seen that for periods smaller than 0.65 sec (columns larger than 65x65 cm), the maximum earthquake demand is given by the Bolu–000 ground motion. For periods between 0.65 sec and 1.20 sec (columns between 40x50 cm and 65x65 cm), the Bolu-090 ground motion governs for larger periods, the maximum drift demand is calculated using DZC-270 and YPT-348. A maximum drift ratio of 6.4% (roof displacement of 45 cm) was calculated for buildings with smaller column sizes.

In the case of stiff soil/rock (Figure 4.10), SKR ground motion controls the maximum drift demand, reaching a maximum value of 2.5% drift ratio (17.5

cm) for the column with cross section of 45x45 cm. In general, the soft soil sites caused much higher drift demands in the idealized buildings.

In order to compare the earthquake demand with the column capacities, it is appropriate to work with boundaries for the earthquake demand. Therefore, maximum, minimum, and average drift ratios are plotted in Figures 4.11 and 4.12 for the two classes of soil. The mean drift demand for soft soil (Figure 4.11) for the different column sizes ranges from 0.5% up to 4.3% (3.5 cm to 30 cm). For the stiff soil/rock sites (Figure 4.12), the mean earthquake demand ranges from 0.2% up to 1.6% (1.5 cm to 11 cm).

Table 4.2 Earthquake Demand Drift Ratios (ζ=2%)

Ground Motion Record	**DRIFT RATIOS (%) (ζ=2%)** **Period (sec)** (Cracked Section) **							
	1.56	**1.48**	**1.32**	**1.25**	**1.13**	**1.07**	**1.03**	**0.99**
BOL000 *	3.0	2.8	2.5	2.5	2.8	3.2	3.3	3.2
BOL090*	2.9	3.3	4.2	4.5	4.9	5.0	4.8	4.8
DZC180*	3.5	3.1	2.2	2.2	2.4	2.4	2.1	2.2
DZC270*	5.6	5.0	6.4	6.1	2.7	2.9	3.3	3.6
ARC000	0.5	0.6	0.7	0.7	0.6	0.5	0.5	0.5
ARC090	1.1	1.1	0.9	0.9	0.6	0.5	0.5	0.5
DZC180	2.7	2.6	1.6	1.6	1.7	2.1	1.9	1.7
DZC270	5.0	5.2	4.8	4.3	3.2	3.1	3.0	2.8
GBZ000	1.7	1.6	1.1	0.8	0.7	0.7	0.9	1.1
GBZ270	1.1	0.9	1.1	1.2	0.7	0.9	0.9	0.8
IZT090	2.1	2.0	1.6	1.4	1.2	1.2	1.3	1.3
IZT 180	2.4	2.1	1.4	1.2	1.0	1.5	1.8	1.6
SKR090	2.4	2.1	2.5	2.5	2.3	2.1	1.8	1.7
YPT330	5.3	6.2	4.7	3.5	2.9	2.2	2.1	1.7
YPT348	5.5	6.3	5.3	4.5	3.0	2.2	1.8	1.5

* Düzce earthquake (Nov 12, 1999)

The other motion records correspond to Kocaeli earthquake (Aug 17,1999)

** For the relationship between Period and Column dimensions see Table 4.1

Table 4.2 Earthquake Demand Drift Ratios (ζ=2%) (Cont.)

Ground Motion Record	**DRIFT RATIOS (%) (ζ=2%)** **Period (sec)** (Cracked Section) **								
	.90	**.86**	**.76**	**.74**	**.64**	**.56**	**.45**	**.37**	**.31**
BOL000 *	3.1	2.8	2.3	2.1	2.1	2.7	1.6	0.9	1.1
BOL090*	4.5	4.2	3.2	3.1	1.8	1.8	1.1	0.8	0.5
DZC180*	2.5	2.6	2.5	2.4	1.5	1.5	1.3	0.9	0.6
DZC270*	3.7	3.6	3.2	3.0	1.8	1.4	0.7	0.9	0.5
ARC000	0.4	0.6	0.4	0.4	0.2	0.3	0.2	0.1	0.1
ARC090	0.7	0.7	0.4	0.4	0.2	0.2	0.1	0.2	0.1
DZC180	1.5	1.5	1.2	1.1	1.3	1.2	0.7	0.6	0.3
DZC270	2.0	1.7	1.3	1.3	1.0	0.9	0.7	0.8	0.4
GBZ000	1.2	1.1	0.7	0.5	0.8	0.7	0.5	0.3	0.2
GBZ270	0.4	0.4	0.5	0.4	0.3	0.5	0.5	0.2	0.2
IZT090	1.1	0.9	0.7	0.7	0.9	0.5	0.3	0.3	0.4
IZT 180	1.0	0.8	0.5	0.5	0.6	0.8	0.4	0.2	0.3
SKR090	1.3	1.5	1.1	1.2	0.6	0.8	0.4	0.5	0.4
YPT330	1.6	1.6	1.8	1.6	1.0	0.8	0.6	0.4	0.3
YPT348	1.5	1.7	1.8	1.5	1.1	0.7	0.7	0.4	0.3

* Düzce earthquake (Nov 12, 1999)

The other motion records correspond to Kocaeli earthquake (Aug 17,1999)

** For the relationship between Period and Column dimensions see Table 4.1

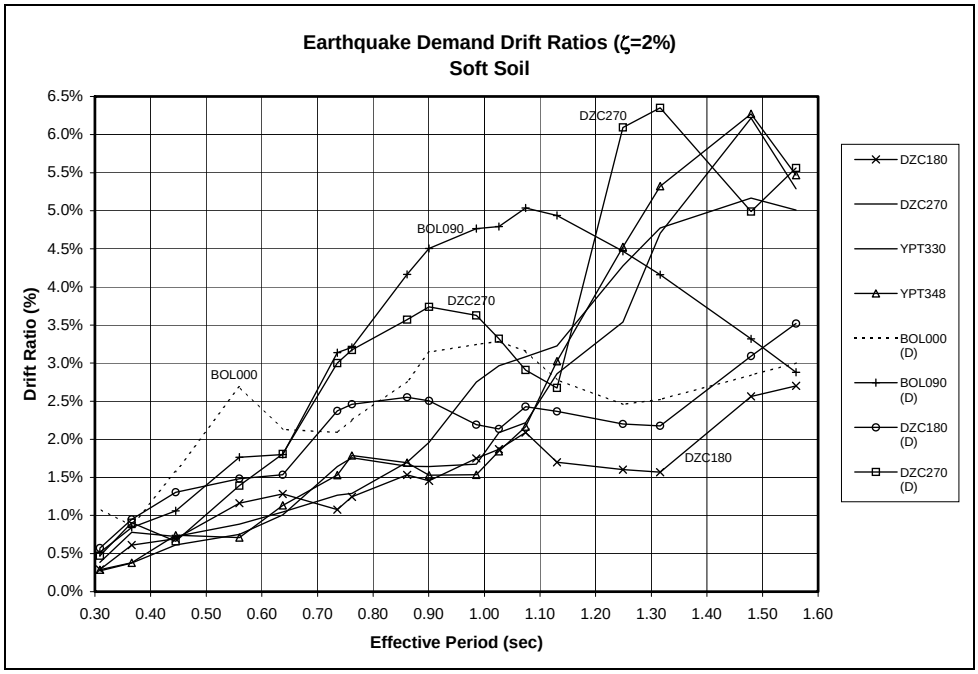

Figure 4.9 Earthquake Demand Drift Ratios vs. Period (Soft Soil)

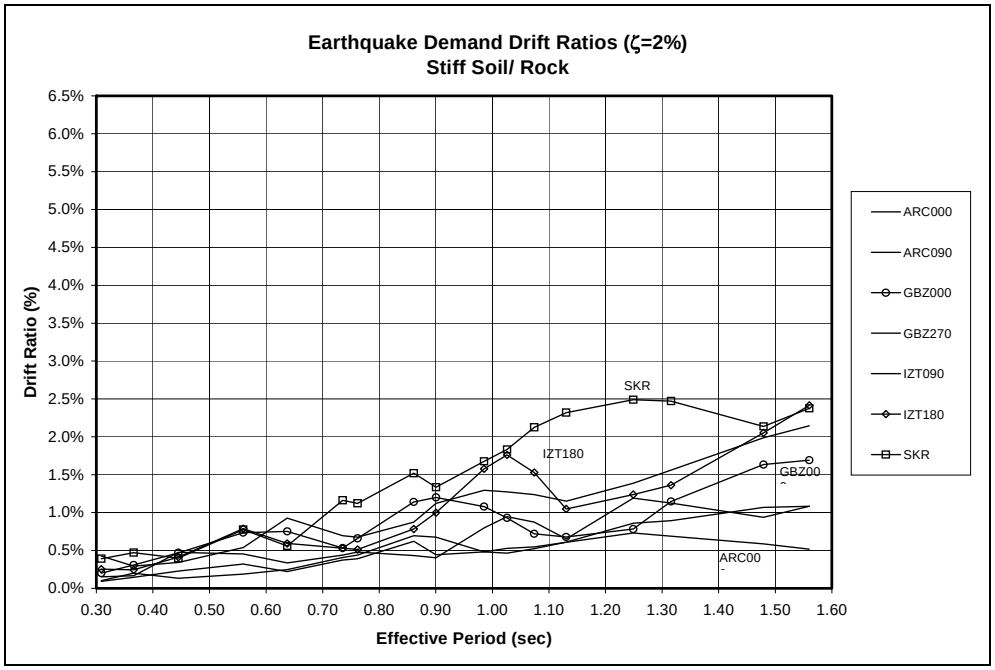

Figure 4.10 Earthquake Demand Drift Ratios vs. Period (Stiff Soil/ Rock)

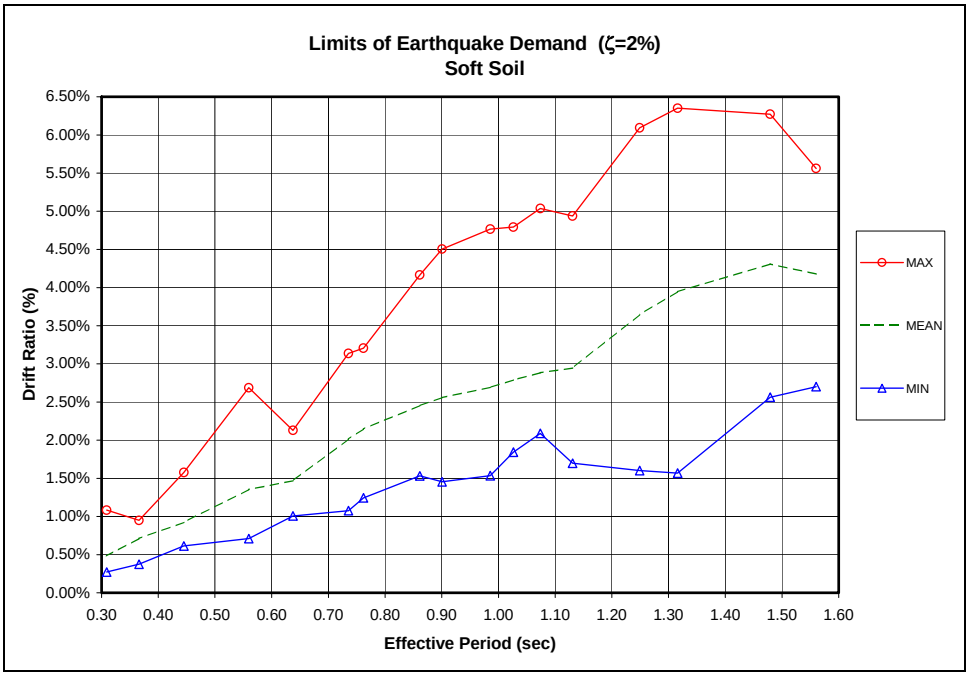

Figure 4.11 Limits of Earthquake Demand for Soft Soil Sites)

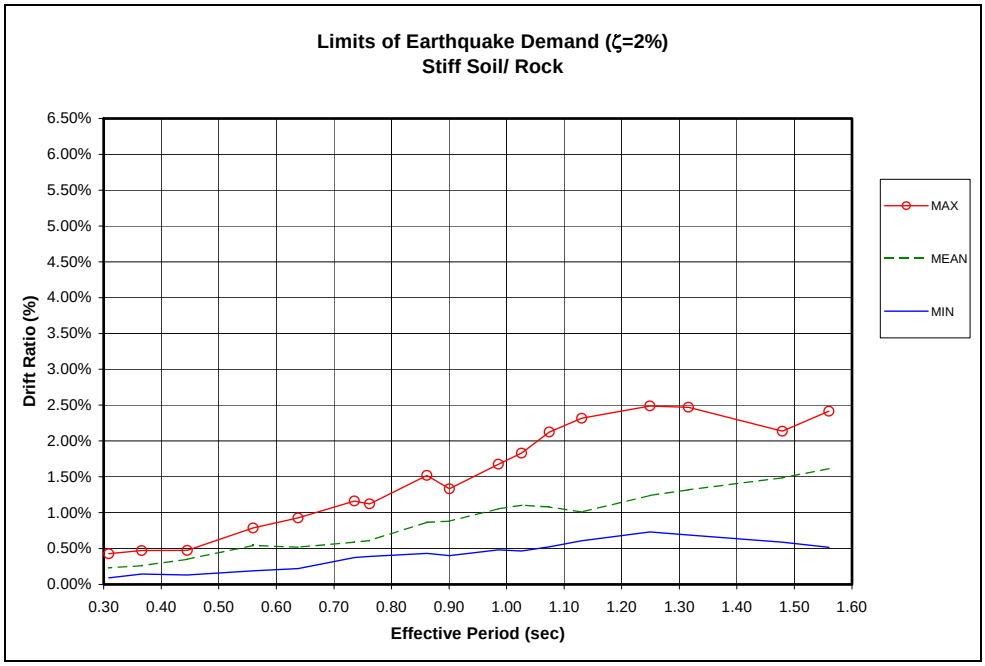

Figure 4.12 Limits of Earthquake Drift Demand for Stiff Soil/Rock Sites

4.5 COLUMN CAPACITIES

The columns in the idealized buildings were studied using three longitudinal reinforcement ratios: ρ = 1%, 2% and 3%, where ρ, the reinforcement ratio, is defined as the ratio of the total area of steel to the gross cross- sectional area of the concrete. The assumed distribution of the reinforcing steel is illustrated in Figure 4.13. Three layers are used for the columns with ρ = 1%, and five layers for ρ = 2 and 3%. It is important to point out that the transverse reinforcement provides negligible confinement of the concrete core because the ties were typically fabricated using 90º hooks. Therefore, the concrete was assumed to be unconfined in all analyses.

The steel reinforcement was idealized using an elasto-plastic model with strain hardening (Figure 4.14). The yield stress was assumed to be 420 MPa and the tensile strength was assumed to be 500 MPa. Strain hardening was assumed for strains exceeding 1%. The modulus of elasticity was assumed to be 204,000 MPa.

The stress-strain relationship for the concrete is based on the Hognestad model (Hognestad, 1951) in which a parabolic curve describes the ascending branch and the descending branch is a straight line (Figure 4.15). The compressive strength of the concrete was assumed to be 30 MPa and the modulus of elasticity was assumed to be 26,000 MPa. The sensitivity of calculated displacement capacity to the ultimate strain in the concrete, ε_{cu}, was evaluated using three values for ε_{cu}: 0.003, 0.0035, and 0.0040. In addition, the deterioration of concrete strength and stiffness with cycling was neglected.

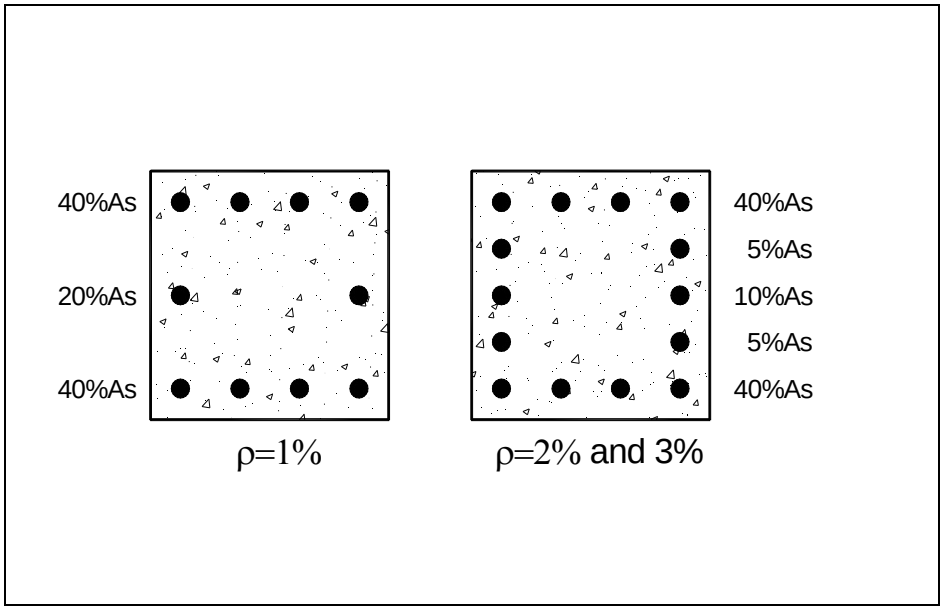

Figure 4.13 Reinforcement Distribution in the Idealized Columns

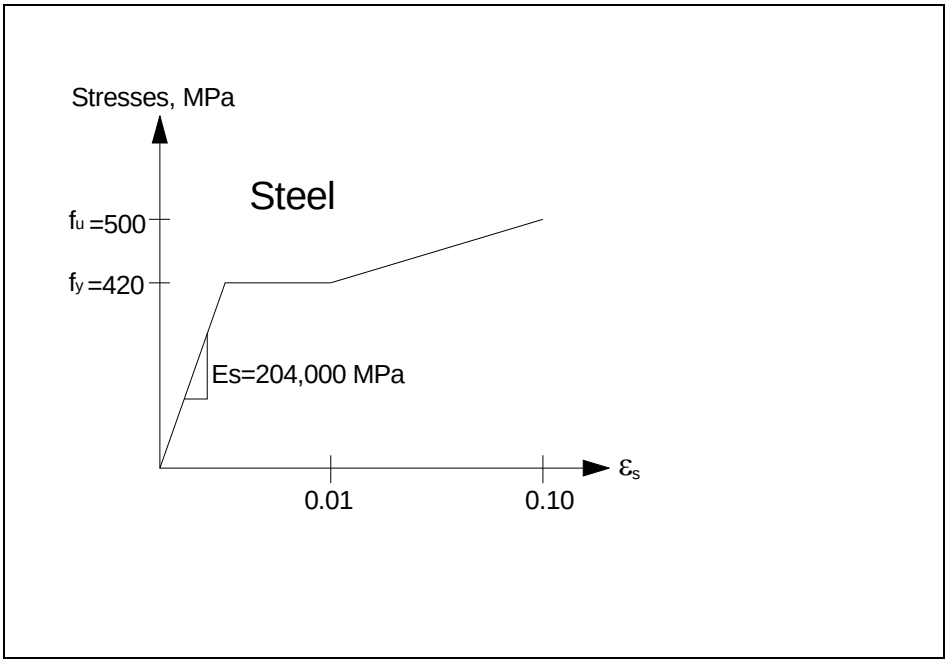

Figure 4.14 Steel Model Used for the Idealized Columns

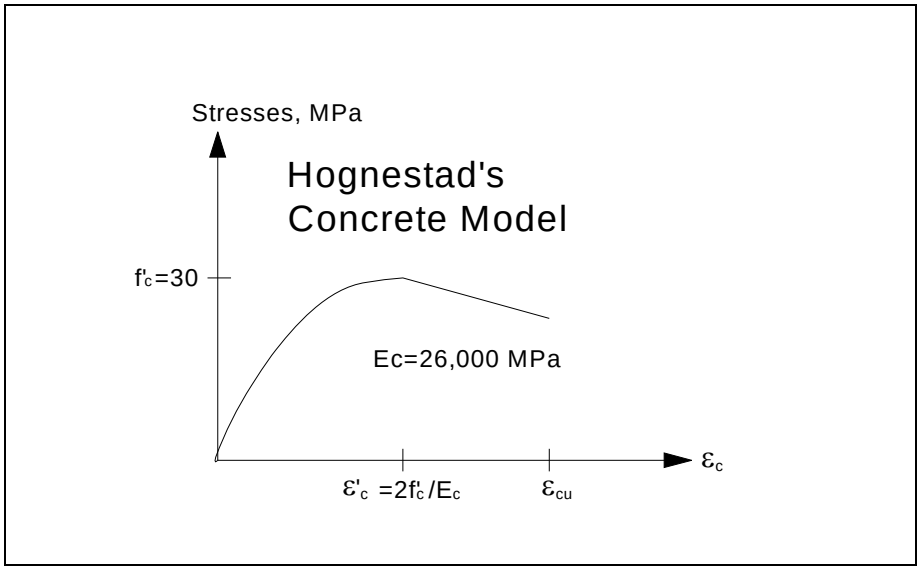

Figure 4.15 Concrete Model Used for the Idealized Columns

Moment-curvature analyses of the idealized columns were computed with the 17 column cross-sections and the three reinforcement ratios. The complete results are presented in Appendix C. The roof displacements corresponding with yielding of reinforcement and capacity of the column were calculated using the results of the moment-curvature analyses, as shown in Figure 4.16.

It is assumed that under the action of small lateral load, the column yields in flexure at the base (Moehle, 1992). This flexural deformation could be modeled by elastic curvature over the height (Figure 4.16) and inelastic curvature concentrated along a plastic hinge of equivalent length l_p at the base. Applying moment-area theorems, the yield displacement Δ_Y and the displacement capacity Δ_U, can be obtained, as expressed in Equations 4.2 and 4.3, respectively.

In Equations 4.2 and 4.3, ϕ_y is the yield curvature, L is the column height and ϕ_U is the curvature capacity. The equivalent plastic hinge, l_p, in a reinforced concrete member (Moehle, 1992) depends on different parameters such as the

section depth, aspect ratio, reinforcing bar diameter, and the magnitudes of the axial and shear loads. Moehle (1992) suggests that the plastic hinge length may be assumed to be *lp* = 0.5 *h*, where *h* is the section depth. Given the photographic evidence shown in Figures 2.6 and 2.7 this is likely to be a lower bound to the actual plastic hinge lengths. Finally, Δ_y and Δ_U, the yield and displacement capacity, are divided by the column height, L, to obtain the drift ratios at yield and capacity.

$$\Delta_Y = \phi_y \cdot L \cdot \frac{1}{2} \cdot \frac{2L}{3} = \phi_y \cdot \frac{L^2}{3} \qquad \textbf{Equation 4.2}$$

$$\Delta_U = \Delta_y + (\phi_u - \phi_y) \cdot l_p \cdot (L - \frac{l_p}{2}) \qquad \textbf{Equation 4.3}$$

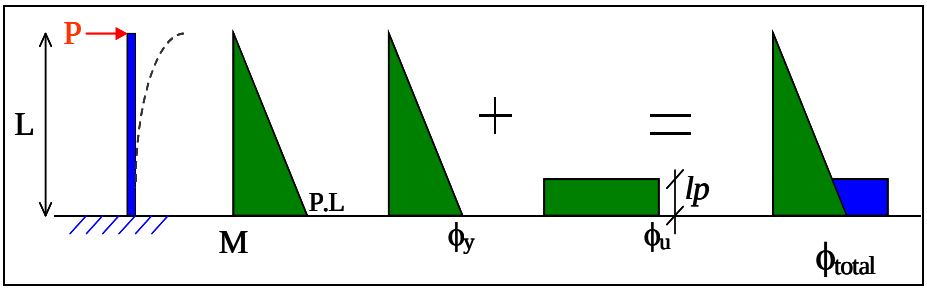

Figure 4.16 Displacement at the Top of the Column Using Moment-Curvature Relationships and Moment-Area Theorem

Tables 4.3, 4.4 and 4.5 summarize the drift ratios corresponding to yield and capacity. Figures 4.17 and 4.18 illustrate the influence of the longitudinal reinforcement ratio (for a fixed value of ultimate strain) on the yield drift ratio and ultimate drift ratio, respectively. It can be seen in Figure 4.17 that the drift ratio at

yield increases as the longitudinal reinforcement ratio increases. This situation can be explained in terms of the curvature at yield. The larger the amount of steel, the larger the curvature at yield, and therefore, the larger the displacement (see Equation 4.2).

On the other hand, the ultimate drift decreases as the longitudinal reinforcement ratio increases (Figure 4.18). In this case, the curvature at capacity decreases when ρ increases. In other words, the ductility decreases when the reinforcement ratio is increased. Similar plots could be presented with the other two ultimate concrete strains; however the results are similar. In order to analyze the effect of considering different values for the ultimate strain, Figure 4.19 is presented. The larger the ultimate strain taken into consideration, the larger the ultimate drift ratio. This could be explained due to the fact that the ultimate curvature increases as the limiting strain in the concrete increases. The larger ultimate curvature produces a larger displacement at capacity (Figure 4.19).

Table 4.3 Ultimate and Yield Drift Ratios for Columns with ρ=1%

Column Dimensions (cm)		Yield Drift	Ultimate Drift (%)		
b (cm)	h (cm)	(%)	ε_{cu}=0.0030	ε_{cu}=0.0035	ε_{cu}=0.0040
40	40	1.96	2.79	2.99	3.14
45	40	2.01	2.86	3.06	3.21
40	45	1.72	2.62	2.84	3.01
45	45	1.70	2.62	2.84	3.01
40	50	1.53	2.49	2.72	2.90
45	50	1.50	2.49	2.72	2.90
50	50	1.47	2.48	2.71	2.90
55	50	1.48	2.51	2.74	2.93
50	55	1.36	2.42	2.67	2.87
55	55	1.32	2.40	2.65	2.85
55	60	1.23	2.36	2.63	2.84
60	60	1.19	2.34	2.61	2.82
65	65	1.10	2.37	2.66	2.88
70	70	1.00	2.27	2.58	2.83
80	80	0.86	2.24	2.57	2.85
90	90	0.74	2.22	2.58	2.88
100	100	0.67	2.23	2.62	2.95

Table 4.4 Ultimate and Yield Drift Ratios for Columns with ρ=2%

Column Dimensions (cm)		Yield Drift	Ultimate Drift (%)		
b (cm)	h (cm)	(%)	ε_{cu}=0.0030	ε_{cu}=0.0035	ε_{cu}=0.0040
40	40	2.19	2.74	2.91	3.04
45	40	2.15	2.72	2.88	3.02
40	45	1.86	2.47	2.65	2.80
45	45	1.84	2.46	2.64	2.79
40	50	1.66	2.30	2.50	2.67
45	50	1.63	2.29	2.49	2.66
50	50	1.64	2.31	2.51	2.68
55	50	1.61	2.29	2.49	2.66
50	55	1.47	2.18	2.39	2.58
55	55	1.44	2.16	2.37	2.56
55	60	1.33	2.08	2.31	2.51
60	60	1.29	2.06	2.29	2.49
65	65	1.17	1.98	2.23	2.45
70	70	1.09	1.94	2.20	2.43
80	80	0.94	1.86	2.15	2.40
90	90	0.82	1.80	2.12	2.40
100	100	0.74	1.78	2.12	2.43

Table 4.5 Ultimate and Yield Drift Ratios for Columns with ρ=3%

Column Dimensions (cm)		Yield Drift	Ultimate Drift (%)		
b (cm)	h (cm)	(%)	ε_{cu}=0.0030	ε_{cu}=0.0035	ε_{cu}=0.0040
40	40	2.31	2.74	2.89	3.02
45	40	2.28	2.72	2.87	3.00
40	45	1.99	2.47	2.63	2.77
45	45	1.96	2.45	2.61	2.75
40	50	1.73	2.24	2.41	2.57
45	50	1.75	2.27	2.44	2.59
50	50	1.72	2.24	2.41	2.57
55	50	1.72	2.25	2.42	2.58
50	55	1.53	2.09	2.28	2.46
55	55	1.54	2.10	2.29	2.47
55	60	1.39	1.98	2.18	2.38
60	60	1.39	1.99	2.19	2.39
65	65	1.26	1.89	2.11	2.32
70	70	1.15	1.81	2.05	2.26
80	80	0.99	1.70	1.97	2.12
90	90	0.87	1.62	1.91	2.01
100	100	0.78	1.58	1.83	1.94

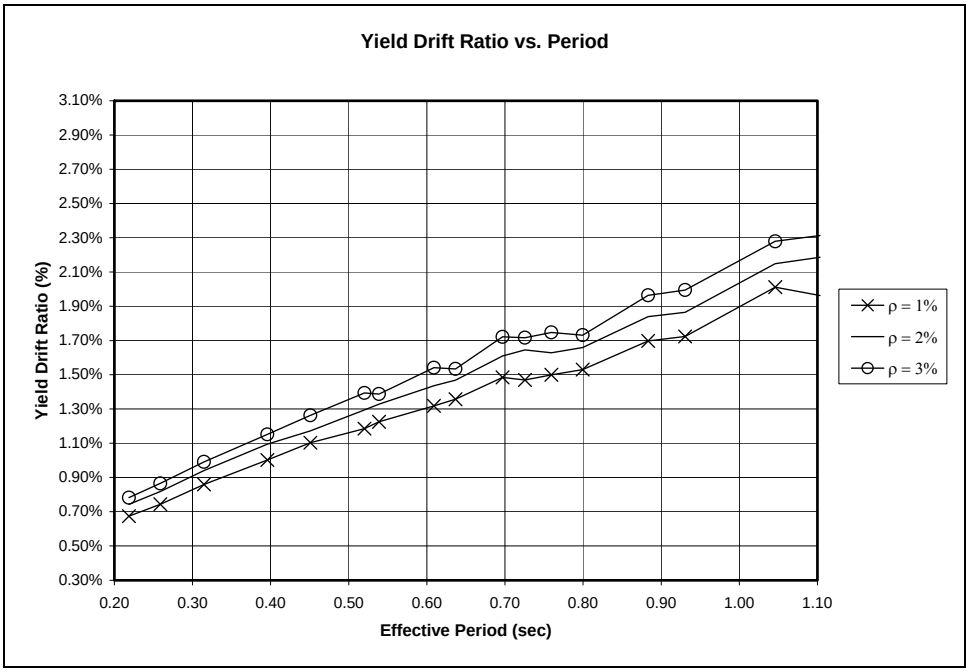

Figure 4.17 Yield Drift Ratio vs. Period

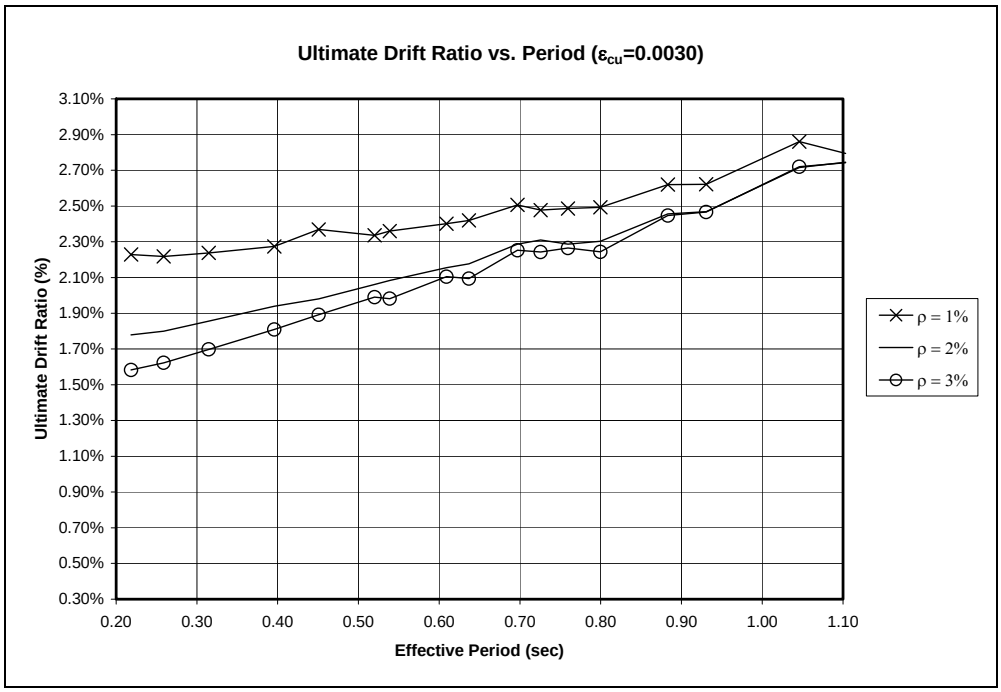

Figure 4.18 Ultimate Drift Ratio vs. Period (ε_{cu}=0.003)

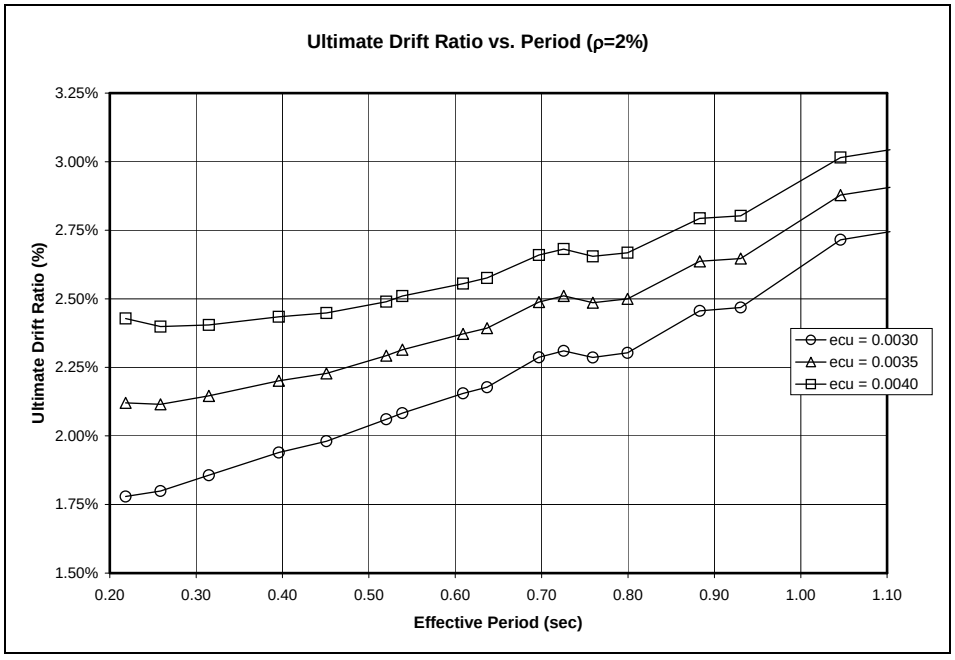

Figure 4.19 Ultimate Drift Ratio vs. Period (ρ=2%)

4.6 DRIFT ANALYSIS

The drift ratios due to the earthquake demand and the drift ratios corresponding to the column capacities were plotted on the same graph in order to detect the critical column sizes. In Figures 4.20 and 4.21, the yield drift ratio is plotted against the effective natural period of the idealized buildings. Some of the column sizes are indicated in the upper part of the graph to assist the reader. The relationship between column size and effective period is reported in Table 4.1. Figures 4.20 (soft soil) and 4.21 (stiff soil/rock) correspond to an ultimate concrete strain of 0.0035.

As illustrated in Figures 4.20 and 4.21, the earthquake demand is plotted as a range with a minimum and a maximum boundary. A mean is also drawn. Some important conclusions can be drawn from the yield drift ratio results for soft soils (Figure 4.20):

- When subjected to the maximum earthquake demand (worst-case scenario), all columns considered in the parametric study will yield.
- Only columns larger than 80 x 80 cm (periods smaller than 0.45 sec) will remain elastic when subjected to the mean earthquake demand.
- Looking at the most optimistic scenario (the minimum earthquake demand), column sizes larger than 55 x 60 cm (periods smaller than 0.76 sec) would remain elastic. The yield drift level in buildings with periods larger than 0.76 sec is approximately equal to the minimum earthquake demand.

The drift analysis observed for the stiff soil/rock sites for a limiting concrete strain of 0.0035 may be summarized as follows (see Figure 4.21):

- The worst-case scenario (maximum earthquake demand) indicates that only columns larger than 55 x 55 cm (periods smaller than 0.86 sec) will remain elastic.
- The minimum and average earthquake demand show that all columns considered in the parametric study will remain elastic.

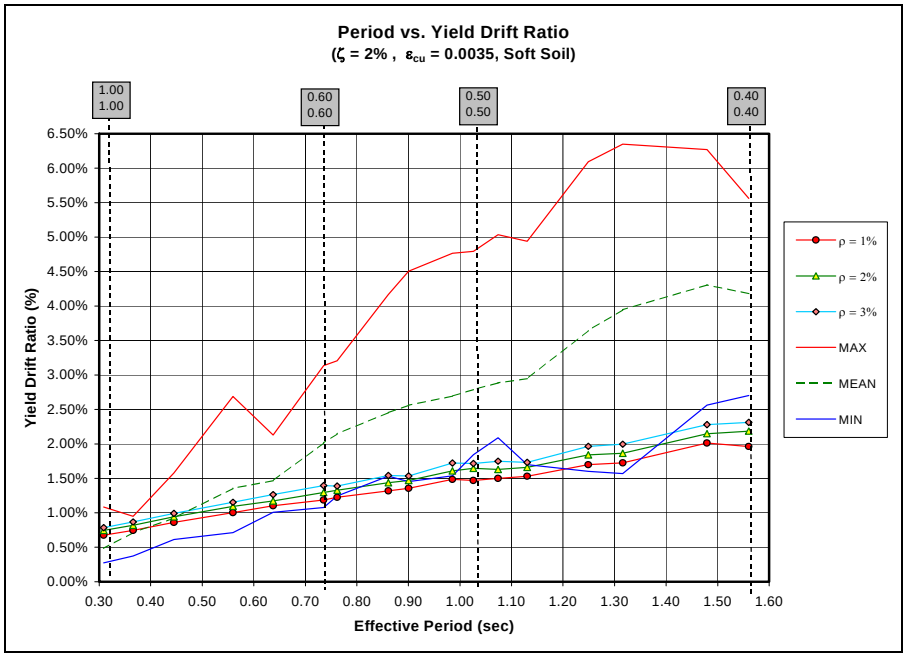

Figure 4.20 Yield Drift Ratio vs. Period (ζ=2%, ε_{cu}=0.0035)(Soft Soil)

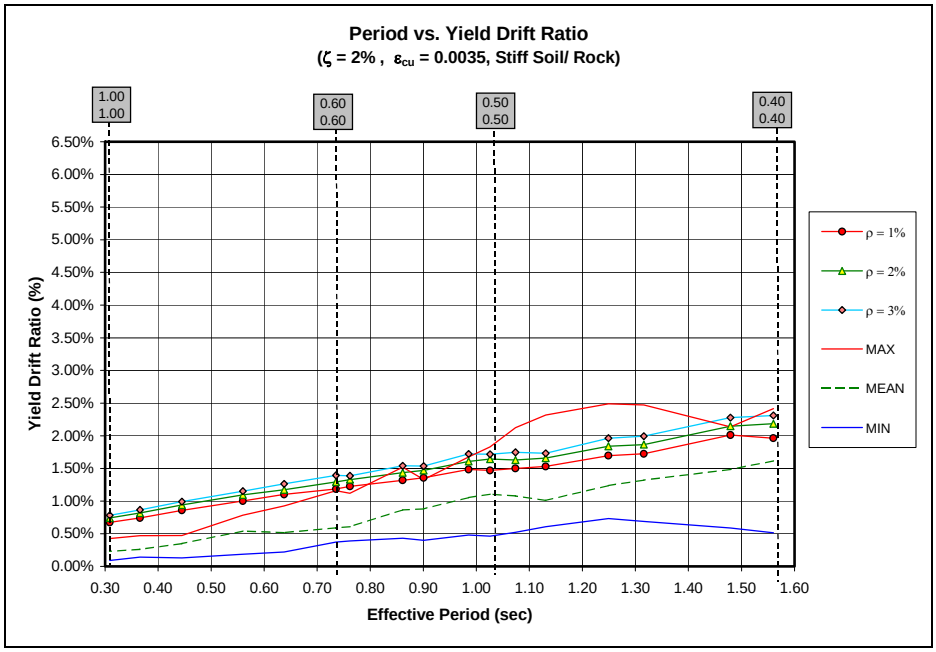

Figure 4.21 Yield Drift Ratio vs. Period (ζ=2%, ε_{cu}=0.0035)(Stiff Soil/Rock)

Similar plots were developed to compare the displacement capacity with the elastic earthquake demand (Figures 4.22 and 4.23). Looking at Figure 4.22 (displacement capacity for soft soil sites), some observations can be made about critical column sizes:

- In terms of the maximum earthquake demand (worst-case scenario), only columns larger than 80 x 80 cm (periods smaller than 0.45 sec) for the three different reinforcement ratios would be able to survive the earthquake.
- Looking at the most optimistic scenario (the minimum earthquake demand), all column sizes considered in the parametric study would survive the earthquake.
- The average case (mean earthquake scenario) indicates that column sizes larger than 55 x 50 cm (periods smaller than 0.99 sec) for $\rho = 1\%$ would survive the earthquake. Similarly, for $\rho = 2\%$ and 3% only columns larger than 55 x 60cm (periods smaller than 0.76 sec) would survive the earthquake.

Figure 4.23 corresponds to displacement capacity vs. period for the stiff soil/rock sites. The following observation can be made:

- All column sizes considered in the parametric study will survive the maximum earthquake demand.

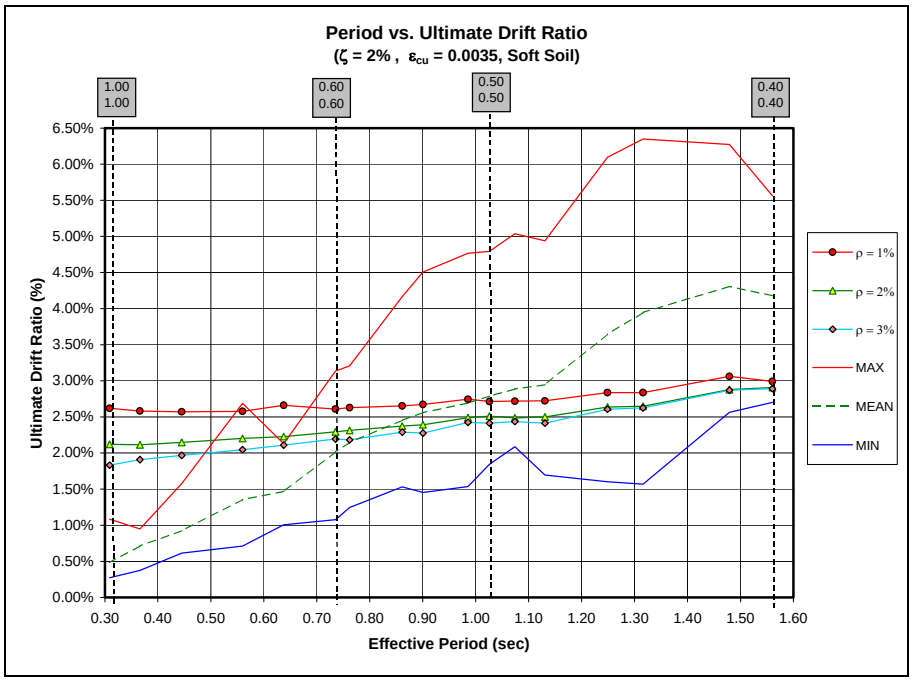

Figure 4.22 Ultimate Drift Ratio vs. Period (ζ=2%, ε_{cu}=0.0035) (Soft Soil)

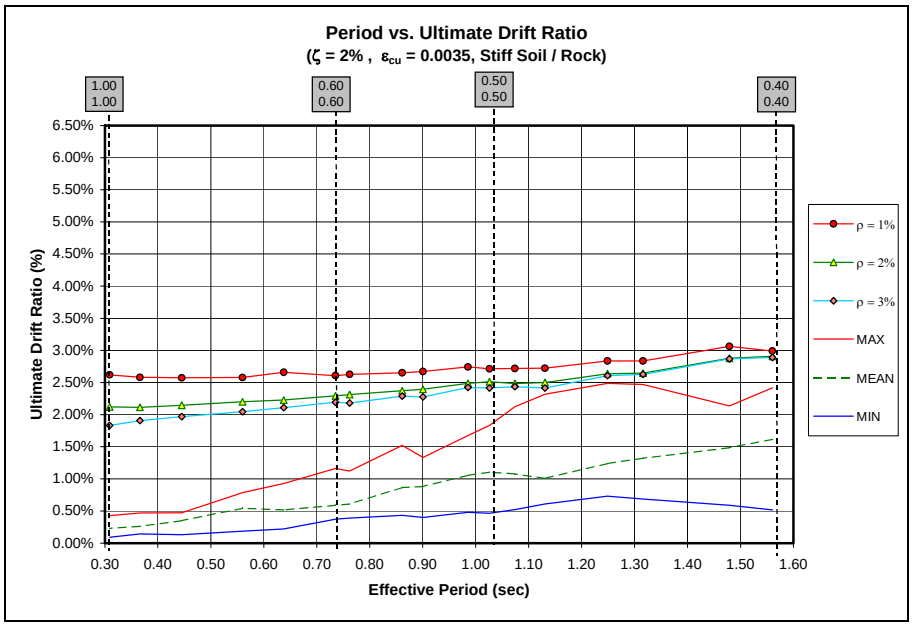

Figure 4.23 Ultimate Drift Ratio vs. Period (ζ=2%, ε_{cu}=0.0035) (Stiff Soil/Rock)

CHAPTER 5
Potential Impact Damage

5.1 DESCRIPTION OF THE PROBLEM

In addition to the problem of the beams unseating due to large drift ratios, an additional source of potential damage was related to rotation of the top of the column. In this typical frame system, the roof girders are very stiff and the columns are flexible; therefore, when the structure is excited by the earthquake, the column rotates and the girder, due to its stiffness, tries to remain horizontal. The consequence of this situation can be observed in Figures 5.1 and 5.2: impact damage near the top of the column. The impact produced spalling of concrete from the roof girder, column or gutter beam. Figures 5.1 and 5.2 illustrate the case where the concrete spalled off the end of the roof girder due to impact, and some of the reinforcement was exposed.

The potential for impact damage is determined by two main parameters as shown in Figure 5.3: the initial gap between the roof girder and the gutter beam, and the height of the gutter beam.

5.2 ANALYSIS OF THE PROBLEM

The maximum rotation before impact can be approximated using Equation 5.1

$$\theta(rad) = \frac{g}{h_g} \qquad \textbf{Equation 5.1}$$

Where g represents the gap distance, h_g is the gutter beam height; and θ is the maximum rotation (in radians) before impact.

Figure 5.1 Concrete's Spalling off Due to Impact when Column Rotates

Figure 5.2 Concrete's Spalling off Due to Impact when Column Rotates

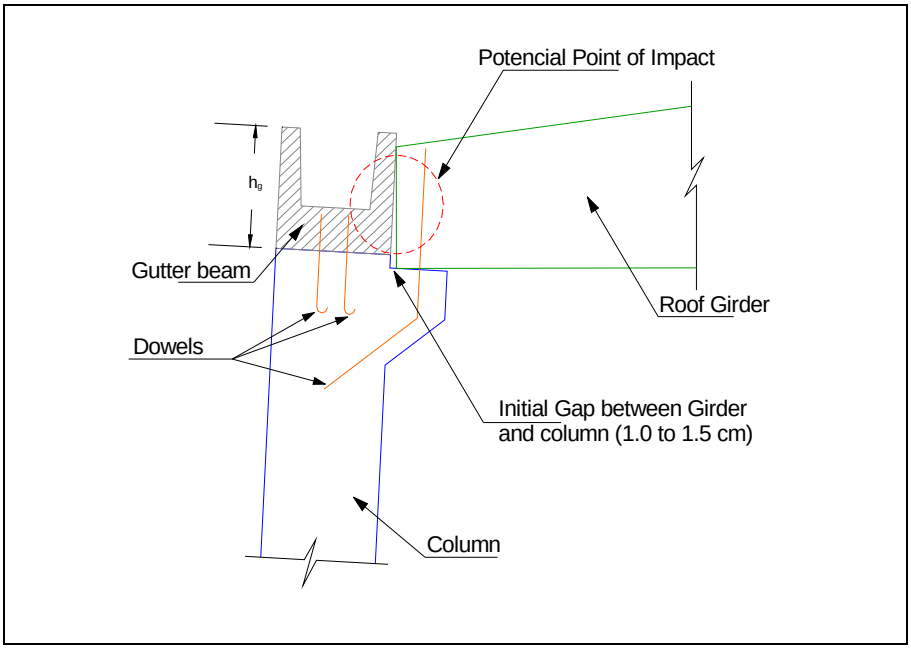

Figure 5.3 Sketch of Potential Impact Problem

Using Equation 5.1, it is possible to plot the ultimate rotation as a function of the effective period in order to detect the critical column sizes. As can be seen in Figures 5.4 and 5.5, two lines can be drawn for the 1 and 1.5-cm gap, because the gutter beam height was fixed as 50 cm and assumed to be independent of the column cross section. The column rotations corresponding to yield and capacity, θ_y and θ_U, can be computed for the three reinforcement ratios, using again the moment-area theorem, as was explained in Chapter 4 (Figure 4.16). Equation 5.2 gives the expression for yield rotation, θ_y and Equation 5.3 for ultimate rotation, θ_U.

$$\theta_y = \phi_y \cdot L \cdot \frac{1}{2} \qquad \textbf{Equation 5.2}$$

$$\theta_U = \theta_y + (\phi_U - \phi_y) \cdot l_p \qquad \textbf{Equation 5.3}$$

Where ϕ_y is the yield curvature, L is the column height and l_p is the plastic hinge length. Figures 5.4 and 5.5 correspond to an ultimate concrete strain of 0.0035.

The following comments can be made about critical column sizes for rotation based on Figures 5.4 and 5.5:

- For a 1-cm gap, columns smaller than 55 x 60 cm (periods larger than 0.76 sec) are expected to impact the adjacent precast member before the longitudinal reinforcement yields (Figure 5.4). However, the larger columns are expected to hit the adjacent precast member after the reinforcement yields, but before the column reaches its flexural capacity (Figure 5.5).
- For the 40 x 40 cm (period =1.56 sec) and 45 x 40 (period=1.48 sec) columns, with 1.5-cm gap; precast members are expected to hit before the longitudinal reinforcement yields (Figure 5.4).
- Figure 5.5 shows that all columns with 1% reinforcement ratio considered in the study are expected to impact before the column reaches its flexural capacity.
- For ρ=2% and 3%, columns smaller than 55 x 55 cm (periods larger than 0.86 sec) are expected to impact before the column reaches its flexural capacity (gap=1.5cm). The larger columns (larger than 55 x 55) will reach their flexural capacity without any impact (Figure 5.5).

In general, the analyses show that larger columns are required to prevent the potential impact damage in this type of structural system.

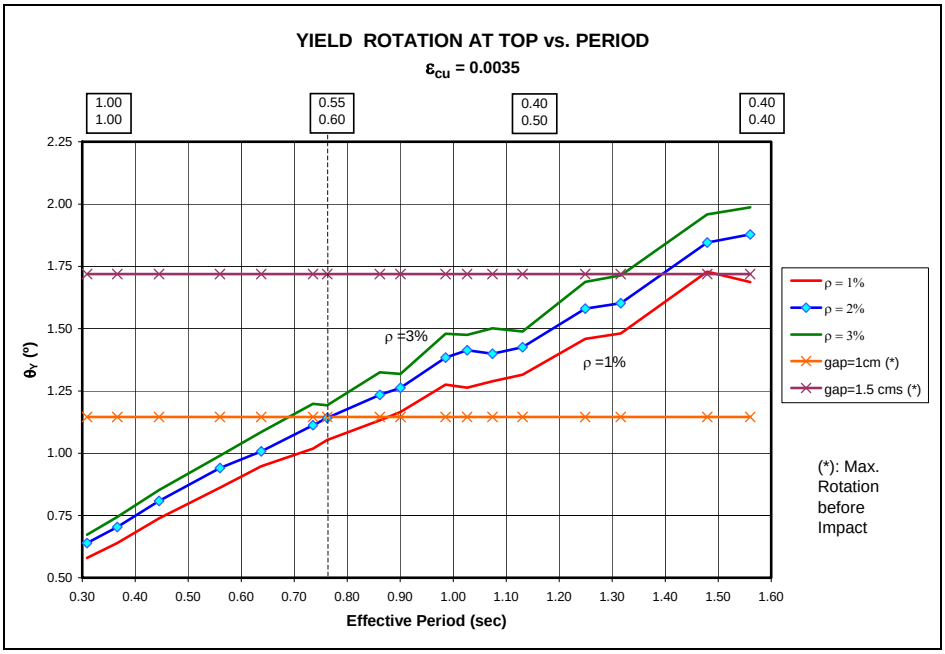

Figure 5.4 Yield Rotation at Top vs. Idealized Building Natural Period

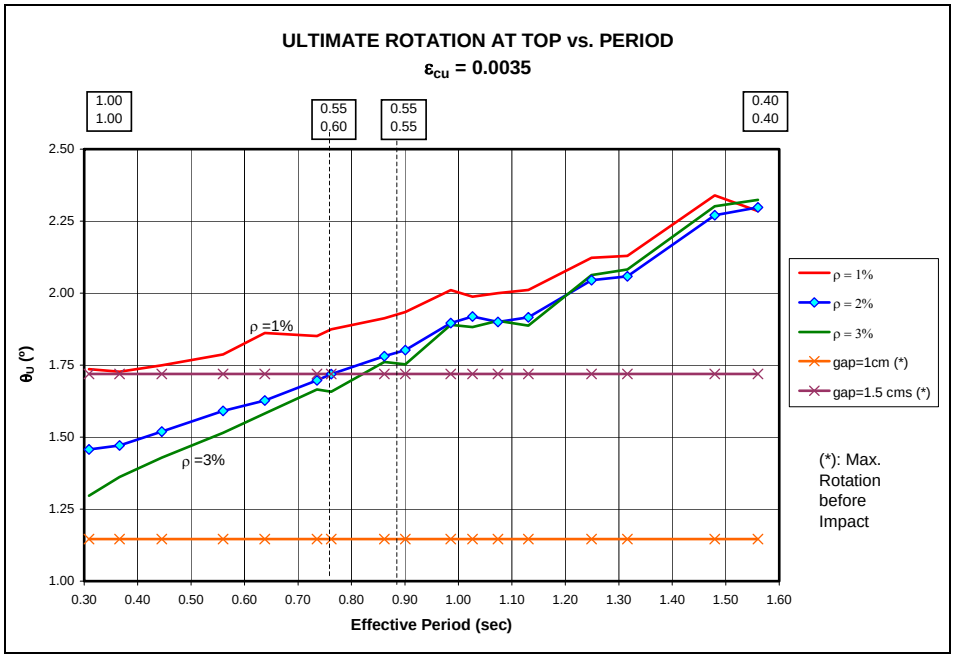

Figure 5.5 Ultimate Rotation at Top vs. Idealized Building Natural Period

CHAPTER 6
Potential for Out-of-Plane Movement of Roof Girders

6.1 PROBLEM DESCRIPTION

Although most of the damage observed in the field was related to movement in the transverse direction (see Chapters 4 and 5), the structural system is also susceptible to damage related to out-of-plane movement of the roof girders. Figure 6.1 clarifies the definition of the longitudinal direction for the structural system taken in the study.

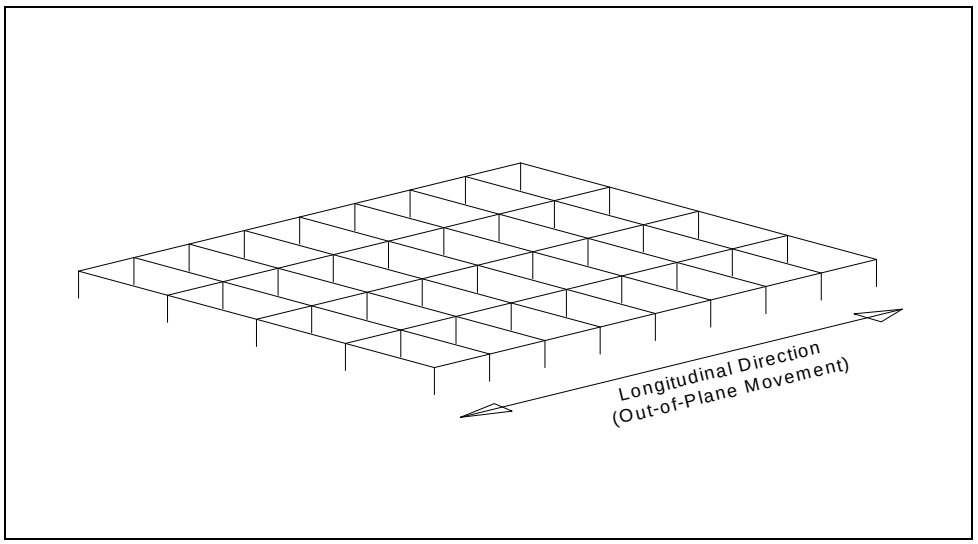

Figure 6.1 Out-of-Plane Direction

When the structure is excited in the longitudinal direction, roof girders could tip over, as shown in Figure 6.2. The concrete corbels, which are reinforced

with steel dowels, are the only structural elements that resist this over-turning moment.

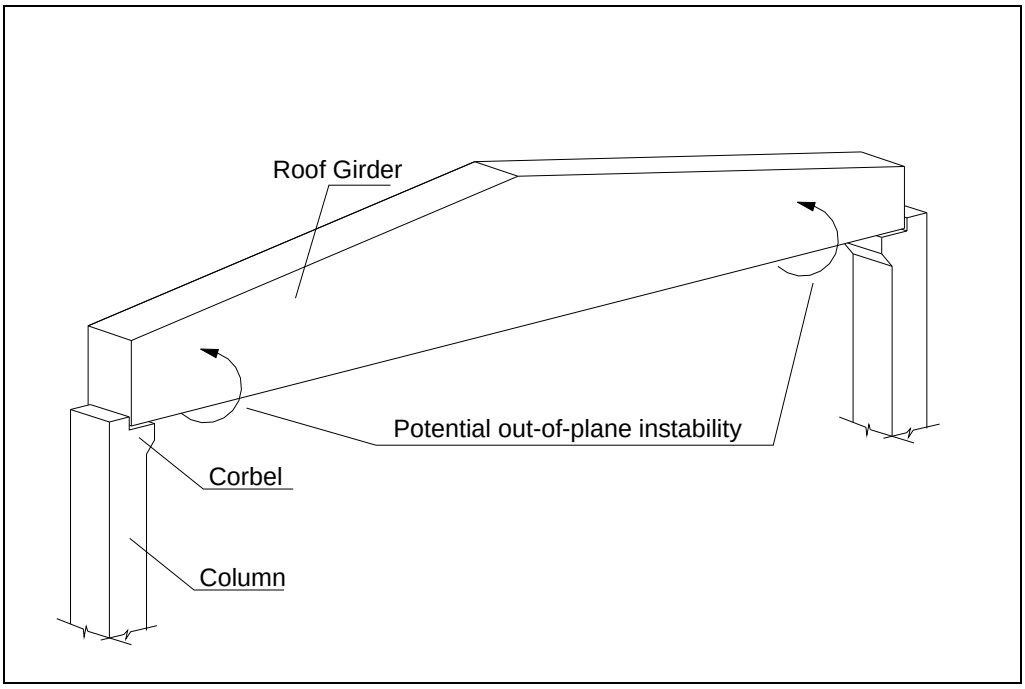

Figure 6.2 Potential Out-of-Plane Instability

6.2 OVERTURNING RESISTANCE OF CORBEL

Figure 6.4 shows the typical corbel detail from the prototype building. The corbel length is fixed at 25 cm, and the width varies depending on the column size (from 40 cm to 100 cm). The reinforcement consists of two, 26-mm diameter steel dowels. The dowels are threaded as shown in Figure 6.3. The length of each dowel is 120 cm. The development length is computed using Equation 6.1, which is the basic development length for a straight deformed bar as specified in ACI-318 (1999).

$$l_{db} = d_b \cdot \frac{f_y \cdot \alpha \cdot \beta \cdot \lambda}{20 \cdot \sqrt{f'_c}}$$ **Equation 6.1**

Where,

f_y = 420 MPa = 30,000 psi f'_c = 30 MPa = 4260 psi

d_b = 26 mm = 1.02 in. α =1.0

β = 1.0 λ = 1.0

Thus, the basic development length, ℓ_{db} is 47 in = 119 cm.

Because the embedment length within the corbel and the embedment length within the girder are both less than the development length of the bar, the maximum stress that can be achieved in the dowels is approximated one-half the yield stress.

Figure 6.3 Threaded Dowels Used as Corbel Reinforcement

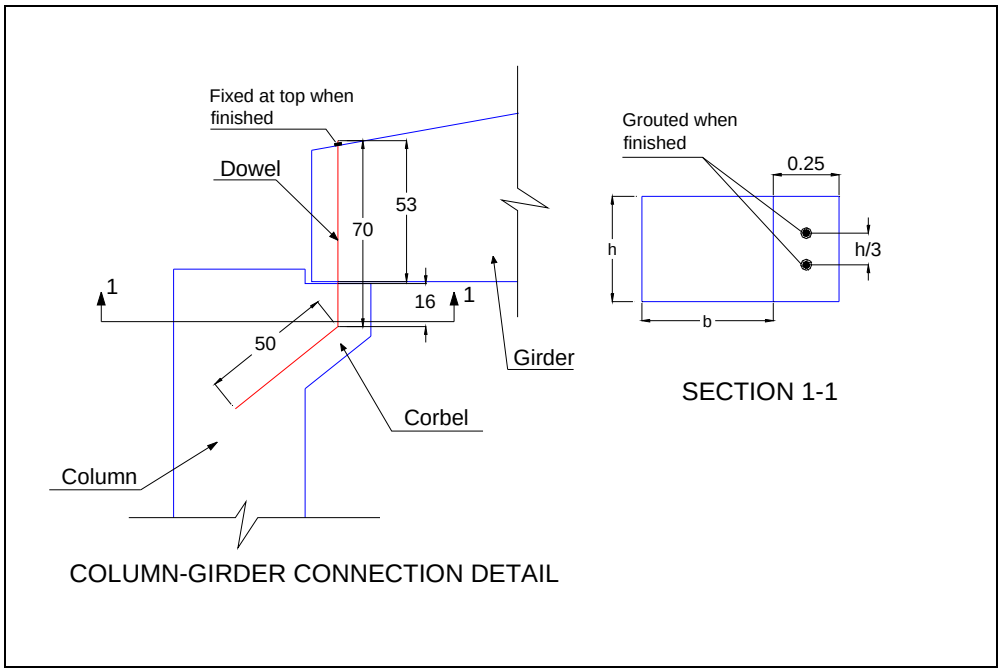

Figure 6.4 Prototype Corbel and Dowel Dimensions

When the construction is finished, the dowels are grouted along their length and a nut is threaded on the top end. Therefore, the fully width of the corbel section is available to resist the overturning moment. A different situation exists when the structure is excited by an earthquake during construction. In this case, the dowels are not working compositely with the concrete in the girder; therefore, only the steel contributes to the overturning resistance of the corbel.

6.2.1 Capacity of Grouted Corbels

Table 6.1 shows the dimensions corresponding to each column size and the resulting flexural capacity.

Table 6.1 Moment Capacity for Grouted Corbels

Column Dimensions (cm)	**Corbel Dimensions (cm)**	**Corbel Capacity (KN-m)**
40 x 40	25 x 40	74.1
45 x 40	25 x 40	74.1
40 x 45	25 x 45	84.6
45 x 45	25 x 45	84.6
40 x 50	25 x 50	95.7
45 x 50	25 x 50	95.7
50 x 50	25 x 50	95.7
55 x 50	25 x 50	95.7
50 x 55	25 x 55	106.9
55 x 55	25 x 55	106.9
55 x 60	25 x 60	118.2
60 x 60	25 x 60	118.2
65 x 65	25 x 65	129.3
70 x 70	25 x 70	140.8
80 x 80	25 x 80	163.6
90 x 90	25 x 90	186.3
100 x 100	25 x 100	209.4

It is also possible to compute the overturning moment demand from the earthquake ground motion. The cases of maximum and mean demand from earthquake motion at sites with soft soil and stiff soil/rock are considered. The force in the structure is calculated by multiplying the roof acceleration by the

average mass of half of the roof girder (in order to compare with the single corbel capacity) (see Figure 4.7). Finally the overturning moment is computed by multiplying this force by the lever arm of 0.36 m, which corresponds to the distance from the centroid of the roof girder to the lower edge. The results of these analyses are summarized in Tables 6.2 and 6.3, and are plotted in Figures 6.5 and 6.6.

Table 6.2 Mean Overturning Moment Demand

T_e* (sec)	Mean Demand Earthquake					
	Roof Acceleration (g)		Force (KN)		Moment (KN-m)	
	Stiff Soil/Rock	Soft Soil	Stiff Soil/Rock	Soft Soil	Stiff Soil/Rock	Soft Soil
1.560	0.19	0.48	8.0	20.2	2.9	7.3
1.316	0.21	0.64	8.9	27.0	3.2	9.7
1.479	0.19	0.55	8.0	23.2	2.9	8.4
1.249	0.22	0.66	9.3	27.8	3.3	10.0
1.414	0.19	0.60	8.0	25.3	2.9	9.1
1.202	0.22	0.63	9.3	26.6	3.3	9.6
1.026	0.30	0.73	12.7	30.8	4.6	11.1
0.901	0.31	0.89	13.1	37.5	4.7	13.5
0.986	0.30	0.78	12.7	32.9	4.6	11.8
0.861	0.33	0.93	13.9	39.2	5.0	14.1
0.849	0.34	0.95	14.1	40.1	5.1	14.4
0.736	0.30	1.04	12.7	43.9	4.6	15.8
0.638	0.36	1.02	15.2	43.0	5.5	15.5
0.560	0.49	1.21	20.7	51.0	7.4	18.4
0.445	0.49	1.29	20.7	54.4	7.4	19.6
0.366	0.54	1.48	22.8	62.4	8.2	22.5
0.309	0.68	1.36	28.7	57.4	10.3	20.7

* Calculated period in the longitudinal direction corresponding to cracked cross-sectional properties

Table 6.3 Maximum Overturning Moment Demand

T_e* (sec)	Maximum Demand Earthquake					
	Roof Acceleration (g)		Force (KN)		Moment (KN-m)	
	Stiff Soil/Rock	Soft Soil	Stiff Soil/Rock	Soft Soil	Stiff Soil/Rock	Soft Soil
1.560	0.28	0.65	11.8	27.4	4.3	9.9
1.316	0.40	1.03	16.9	43.4	6.1	15.6
1.479	0.27	0.81	11.4	34.2	4.1	12.3
1.249	0.45	1.08	19.0	45.6	6.8	16.4
1.414	0.29	0.93	12.2	39.2	4.4	14.1
1.202	0.46	0.91	19.4	38.4	7.0	13.8
1.026	0.49	1.28	20.7	54.0	7.4	19.4
0.901	0.46	1.56	19.4	65.8	7.0	23.7
0.986	0.48	1.37	20.2	57.8	7.3	20.8
0.861	0.58	1.58	24.5	66.6	8.8	24.0
0.849	0.58	1.58	24.5	66.6	8.8	24.0
0.736	0.60	1.62	25.3	68.3	9.1	24.6
0.638	0.60	1.40	25.3	59.1	9.1	21.3
0.560	0.71	2.37	29.9	100.0	10.8	36.0
0.445	0.70	2.20	29.5	92.8	10.6	33.4
0.366	0.97	2.01	40.9	84.8	14.7	30.5
0.309	1.37	2.99	57.8	126.1	20.8	45.4

* Calculated period in the longitudinal direction corresponding to cracked cross-sectional properties

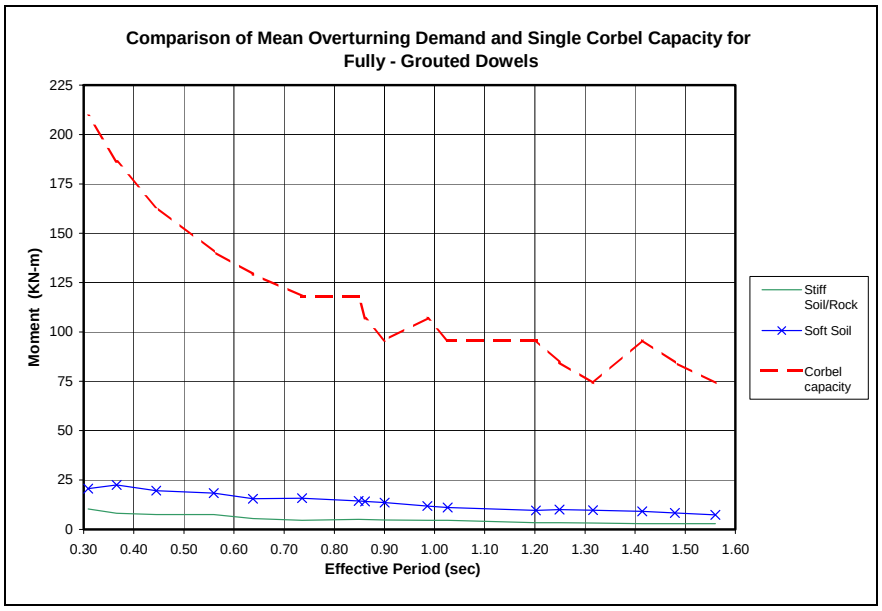

Figure 6.5 Comparison of Mean Overturning Demand and Single Corbel Capacity for Fully-Grouted Dowels

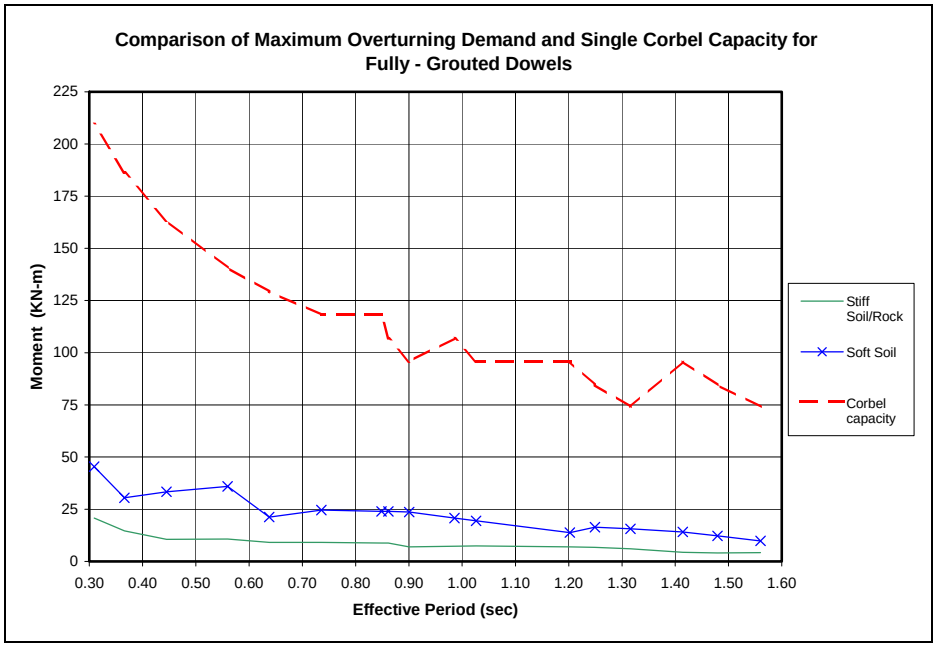

Figure 6.6 Comparison of Maximum Overturning Demand and Single Corbel Capacity for Fully-Grouted Dowels

As shown in Figures 6.5 and 6.6, the resisting capacity of corbels exceeds the earthquake demand. Therefore, for the cases considered, overturning of the roof girders is not expected when construction is completed and the dowels are fully grouted.

6.2.2 Capacity of Corbels when dowels are ungrouted

During construction the dowels are not grouted and the resisting moment is calculated using the steel only (Figure 6.7).

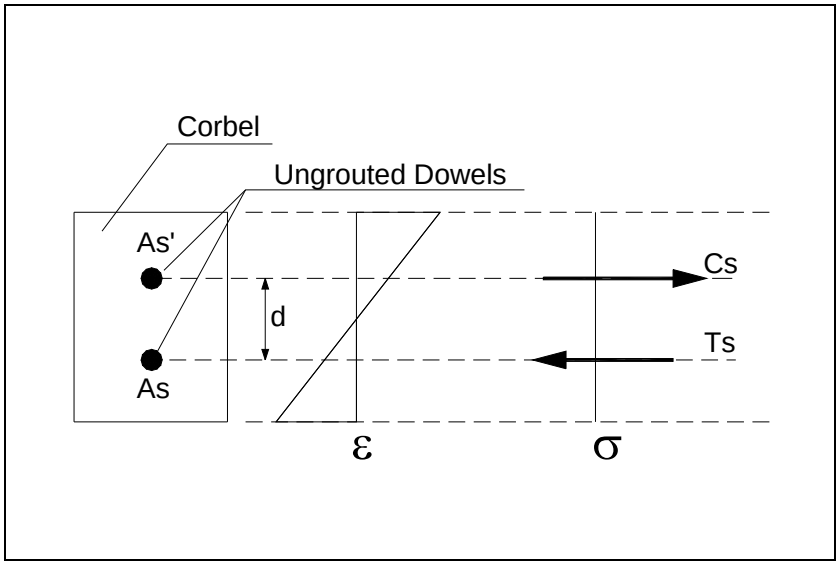

Figure 6.7 Assumed Stresses in Corbel for Ungrouted Dowels

Therefore, the limiting moment is equal to:

$$M = f_s \cdot A_s \cdot \frac{d}{2} + f_s \cdot A_{s'} \cdot \frac{d}{2} \qquad \textbf{Equation 6.2}$$

Where d is the distance between the ungrouted dowels (Figure 6.7) and f_s is the stress in the dowel (assumed to be $f_y/2$). A_s and A_s' are the cross-sectional

areas of the dowels for compression and tension, respectively. Table 6.4 summarizes the results for the case of ungrouted dowels.

Table 6.4 Moment Capacity of Single Corbel with Ungrouted Dowels

Column Dimensions (cm)	**Corbel Dimensions (cm)**	**d (cm)**	**Single Corbel Capacity (KN-m)**
40 x 40	25 x 40	12	13.4
45 x 40	25 x 40	12	13.4
40 x 45	25 x 45	14	15.1
45 x 45	25 x 45	14	15.1
40 x 50	25 x 50	15	16.7
45 x 50	25 x 50	15	16.7
50 x 50	25 x 50	15	16.7
55 x 50	25 x 50	15	16.7
50 x 55	25 x 55	17	18.4
55 x 55	25 x 55	17	18.4
55 x 60	25 x 60	18	20.1
60 x 60	25 x 60	18	20.1
65 x 65	25 x 65	20	21.7
70 x 70	25 x 70	21	23.4
80 x 80	25 x 80	24	26.8
90 x 90	25 x 90	27	30.1
100 x 100	25 x 100	30	33.4

The values of single corbel capacity with ungrouted dowels are plotted in Figures 6.8 and 6.9 with the mean and maximum overturning demand, respectively. The behavior can be summarized as follows:

- When subjected to the mean overturning demand (Figure 6.8), the resisting capacity of the corbel exceeds the earthquake demand. Therefore, overturning of the roof girders is not expected when the dowels are not grouted for this mean overturning moment demand.
- When subjected to the maximum overturning demand (worst-case scenario) (Figure 6.9), the resisting capacity of the corbel exceeds the earthquake demand for stiff soil/rock sites; therefore overturning of the roof girder is not expected in these sites. However, for soft soil sites the overturning moment is greater than the corbel capacity, therefore the roof girder is expected to tip over. This last situation is observed (Figure 6.9) for all corbel sizes considered in the study, and appears to be worse for the larger columns (smaller periods) because forces are related to accelerations, and larger columns lead to larger calculated forces.

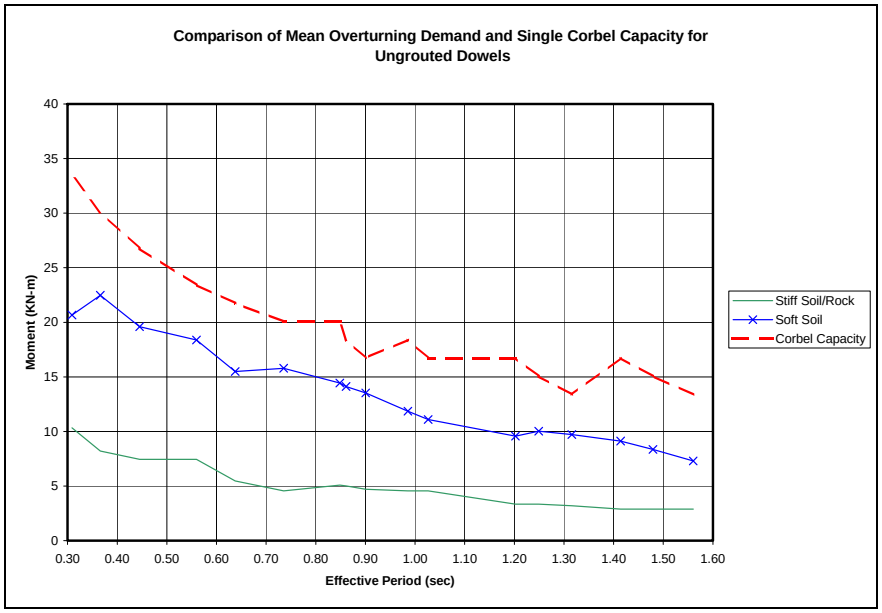

Figure 6.8 Comparison of Mean Overturning Demand and Single Corbel Capacity for Ungrouted Dowels

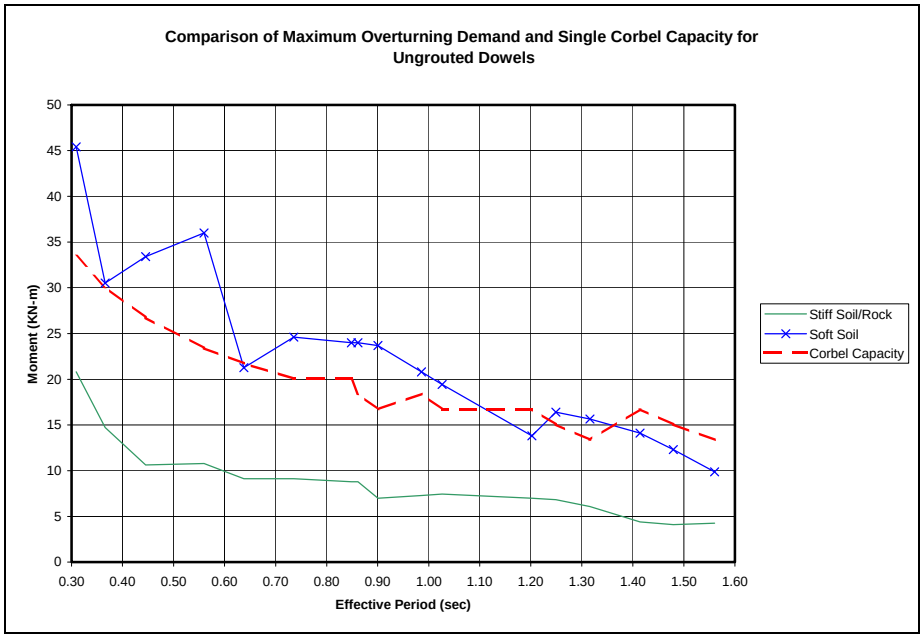

Figure 6.9 Comparison of Maximum Overturning Demand and Single Corbel Capacity for Ungrouted Dowels

CHAPTER 7
Conclusions

The 1999 Kocaeli and Düzce earthquakes caused severe damage to precast buildings. Precast frame buildings are used throughout Turkey for many industrial facilities. One-story industrial buildings are the most common structural system. These systems are economical to construct and provide large open reas for manufacturing. Different structural problems were identified and observed in the field; such as large drift ratios, plastic hinges at the bottom of the columns, out-of-plane movement of the roof girders, and girder-column impact. In many cases large levels of distortion led to unseating of roof girders, and therefore collapse of the roofs.

The thesis has focused on the flexural response of transverse frames of the one-story precast concrete industrial building during the 1999 Turkish earthquakes. A parametric study based on column sizes and the dimensions of a prototype one-story precast concrete building was carried out. Drift capacity, impact damage and out-of-plane rotation of the roof girders were studied by comparing the flexural capacities with the earthquake demand. Three reinforcement ratios (ρ = 1%, 2% and 3%), three values of limiting strain in the concrete (ε_{cu} = 0.0030, 0.0035 and 0.0040), and fifteen ground motion records (eight measured on soft soil and seven on stiff soil/rock sites) were considered.

First, a drift analysis was developed to compare column capacities with earthquake demand. The primary parameter, column size was varied from 40x 40 cm to 100 x 100 cm. All analyses were conducted using cracked cross-sectional properties for the columns. Drift ratios corresponding to yielding of the longitudinal reinforcement and capacity of idealized columns were calculated.

The following conclusions for each one of the scenarios considered (maximum, mean and minimum earthquake demand) are presented:

- Large differences were calculated using ground motions corresponding to soft soil sites compared with the stiff soil/rock sites. On average, drift ratios for soft soils are 2.5 to 3 times larger than those at stiff soils/rock sites.
- Mean earthquake demand: At the soft soil sites, only buildings with columns larger than 60 x 60 cm will survive the earthquake. However, the calculated drift ratio is significant, with more than 2% for structures with columns of this size. At the stiff soil/rock sites, all columns considered in the study would survive the earthquake.
- Minimum demand earthquake (optimistic scenario): All structures considered in the study would survive the earthquake. However, the buildings with columns smaller than 40 x 45 cm will experience yielding of the longitudinal reinforcement.
- Maximum demand earthquake (worst-case scenario): For soft soils, only columns larger than 80 x 80 cm will survive the earthquake. For stiff soil/rock sites, all columns considered in the study would withstand the earthquake; however, only columns larger than 55 x 55 cm would remain elastic.
- The results are not sensitive to the longitudinal reinforcement ratio or the limiting strain in the concrete.
- In general, drift must be controlled for this type of structural system to survive future earthquakes. Small columns should be avoided in order to survive future earthquakes, and larger columns are required if the soil conditions are poor. The writer suggests that columns smaller than

60 x 60 cm in this particular type of structural system represent a high risk of collapses during a severe earthquake and therefore, should be avoided.

Potential impact damage between the roof girder and the column or gutter beam was studied. The girders are very stiff and the columns are quite flexible. Therefore, when the structure is excited by the earthquake, the column rotates and the girder, due to its stiffness, tends to remain horizontal; producing the subsequent impact. Two different values of gap distance between the girder and the gutter beam were considered (1 cm and 1.5 cm). The following conclusion can be made about critical column size:

- In general, the analyses show that larger columns are required to prevent the potential impact damage in this type of structural system. In addition, providing a larger gap distance between the girder and the column/gutter beam is vital. The results showed that increasing the gap from 1 cm to 1.5 cm could have a significant influence on performance.

Potential for out-of-plane movement of roof girders was studied. When the structure is excited in the longitudinal direction, the roof girder could tip over. When the construction is finished, the threaded dowels are grouted along their length and a nut is threaded at the top end. When the structure is excited during an earthquake the dowels are ungrouted. Therefore, only the steel contributes to the corbel capacity. These two situations were taken into consideration and the results are summarized as follows:

- When the construction is completed and the dowels are fully grouted, overturning of roof girders is not expected because the resisting capacity of corbels exceeds the earthquake demand.
- When the structure is excited during construction, the resisting capacity of the corbel exceeds the earthquake demand for stiff soil/rock sites.

Therefore, overturning of the roof girder is not expected at these sites. However, for soft soil sites the overturning moment (maximum demand) is greater than the corbel capacity, and therefore, the roof girder is expected to tip over. In other words, if the structure is located in soils with poor conditions, there is a high risk of out-of-plane movement of roof girders during the construction period, and therefore, the dowels must be fully grouted as soon as possible.

It is important to realize that this parametric study only considered one column height (7 m); however it was observed in the field that this height is very common, and in many cases the story height is larger. Obviously, larger cross-sectional dimensions for the columns would be required to control damage in taller structures.

In general, column dimensions and connection details are considered to have a critical influence on the performance of these types of precast systems during strong earthquakes.

Appendix A

A. 1 ACCELERATION RECORDS FROM KOCAELI EARTHQUAKE

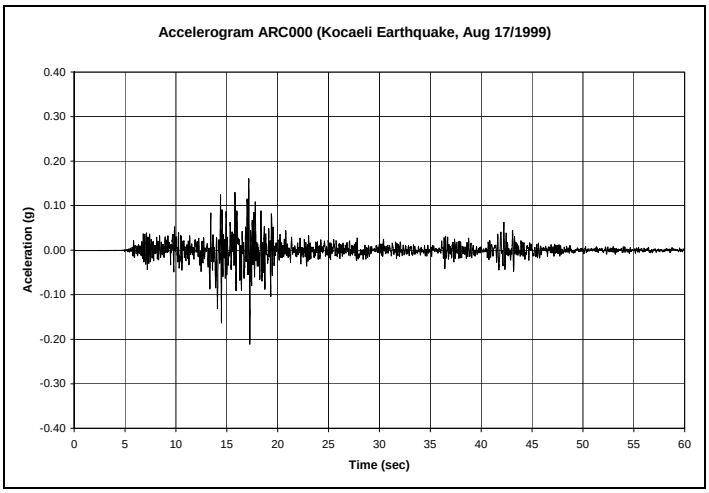

Figure A-1 Accelerations Recorded in Arcelik (000 Component)

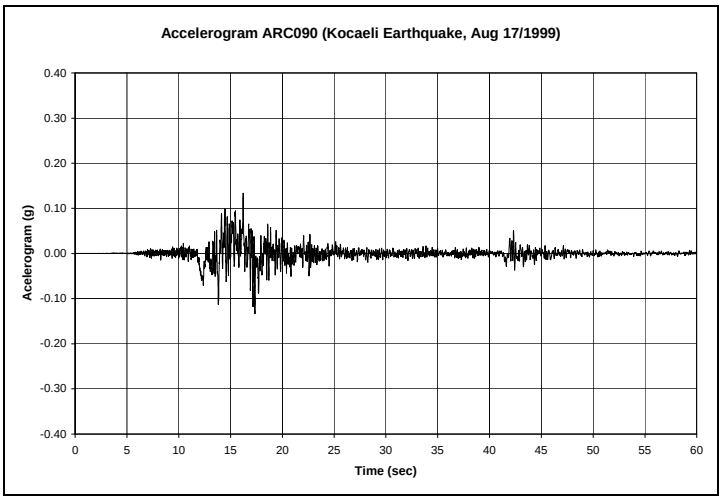

Figure A-2 Accelerations Recorded in Arcelik (090 Component)

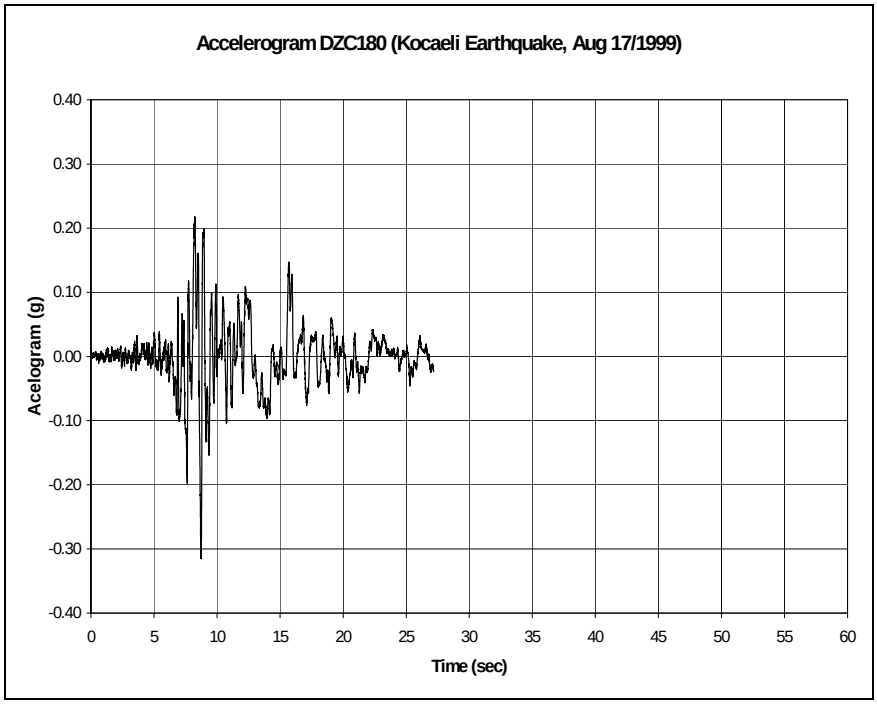

Figure A-3 Accelerations Recorded in Düzce (180 Component)

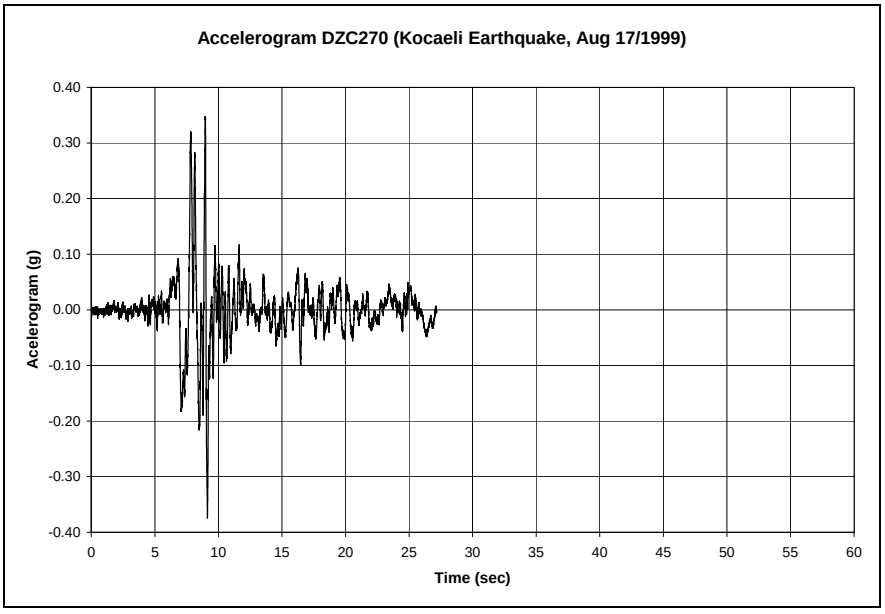

Figure A-4 Accelerations Recorded in Düzce (270 Component)

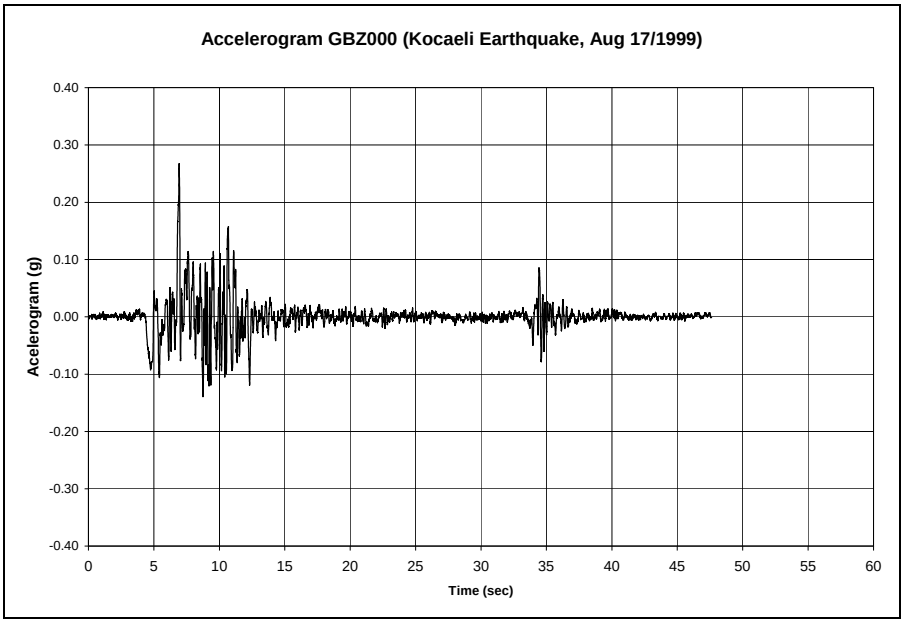

Figure A-5 Accelerations Recorded in Gebze (000 Component)

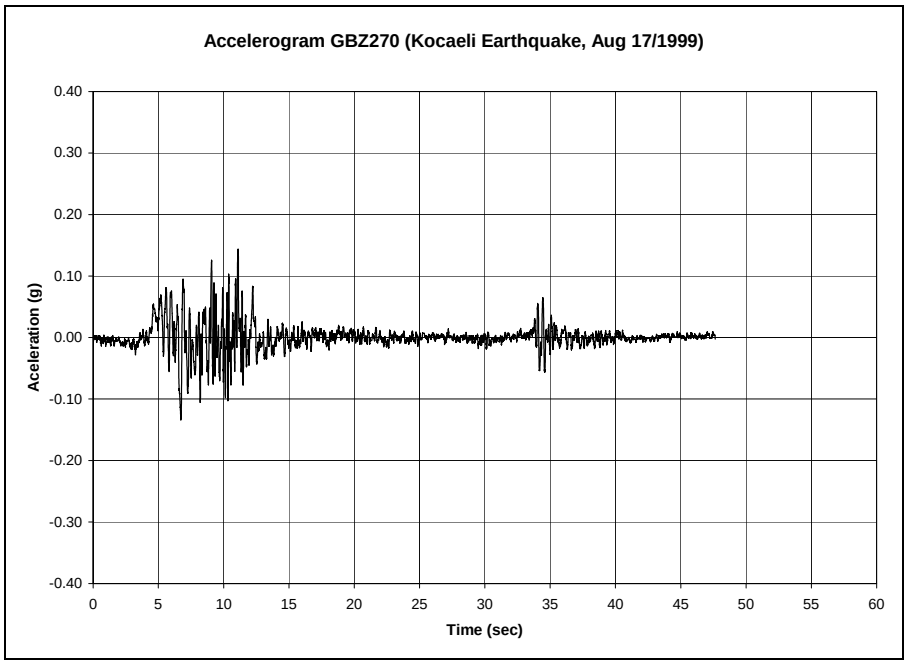

Figure A-6 Accelerations Recorded in Gebze (270 Component)

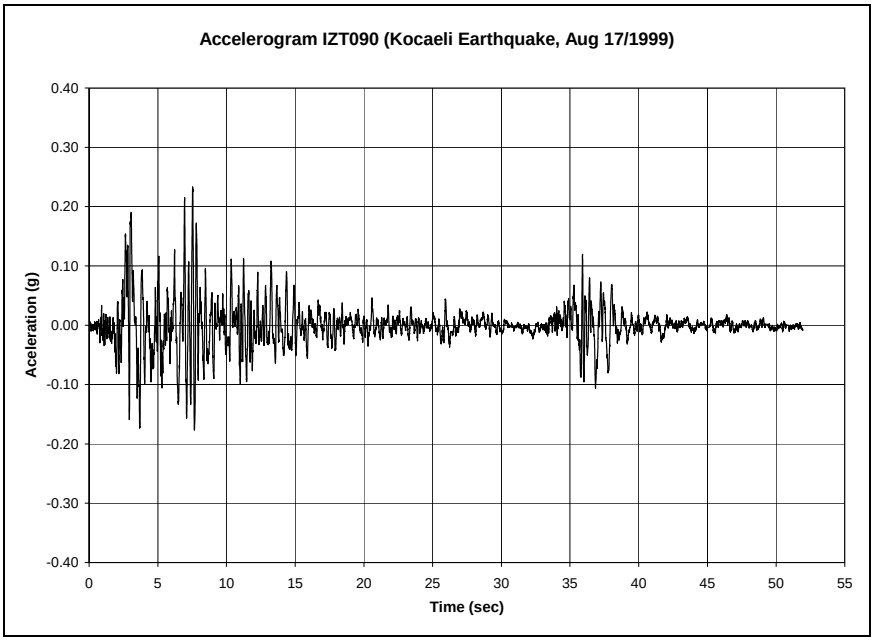

Figure A-7 Accelerations Recorded in Izmit (090 Component)

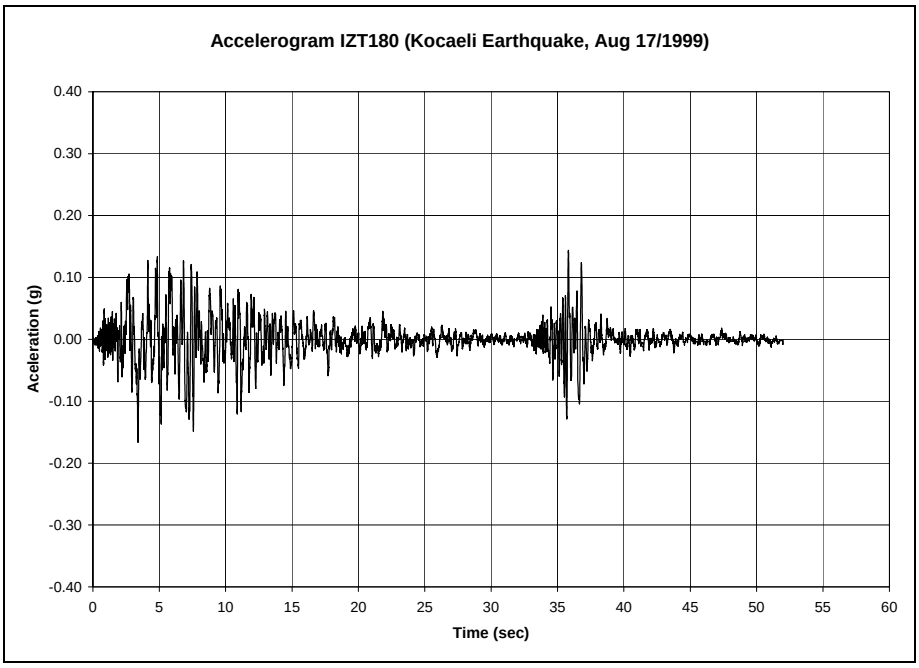

Figure A-8 Accelerations Recorded in Izmit (180 Component)

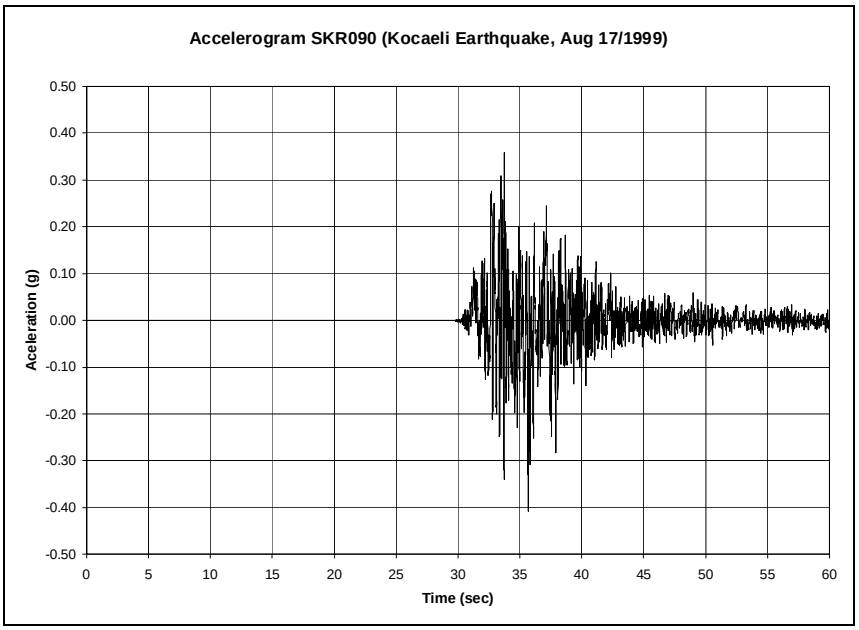

Figure A-9 Accelerations Recorded in Sakarya (090 Component)

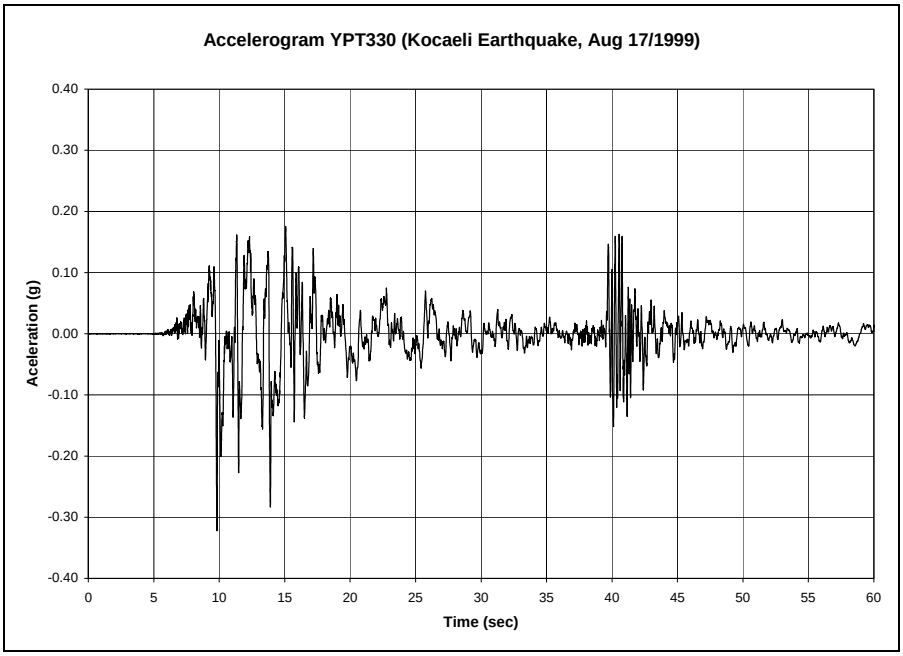

Figure A-10 Accelerations Recorded in Yarimca (330 Component)

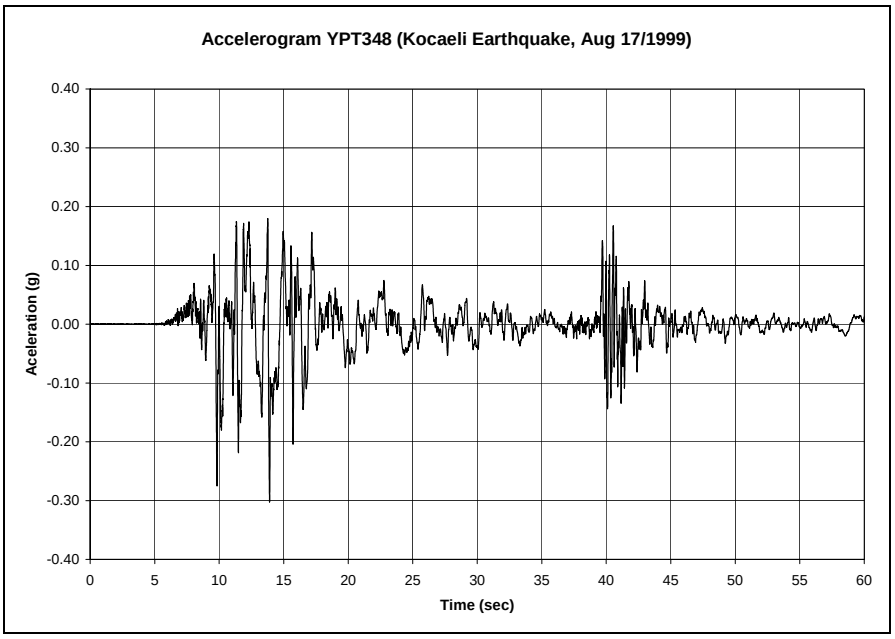

Figure A-11 Accelerations Recorded in Yarimca (348 Component)

A.2 ACCELERATION RECORDS FROM DÜZCE EARTHQUAKE

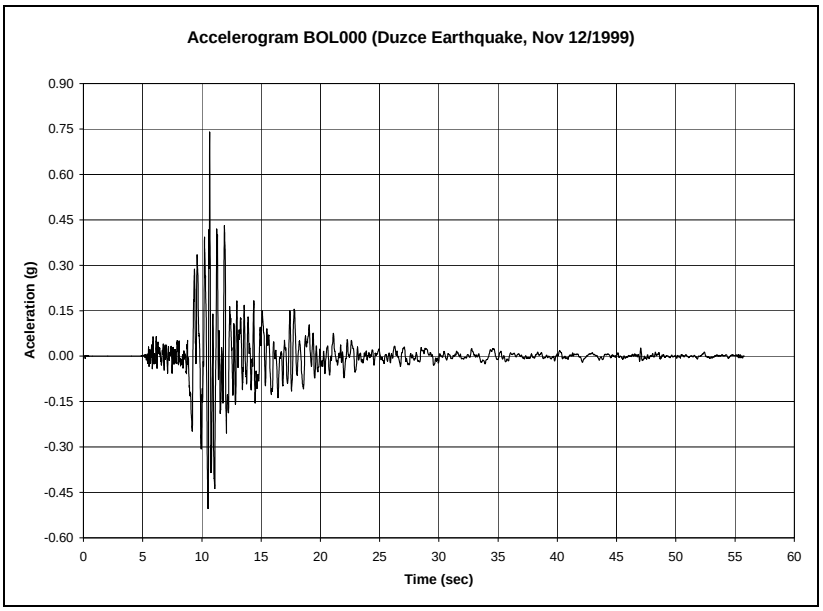

Figure A-12 Accelerations Recorded in Bolu (000 Component)

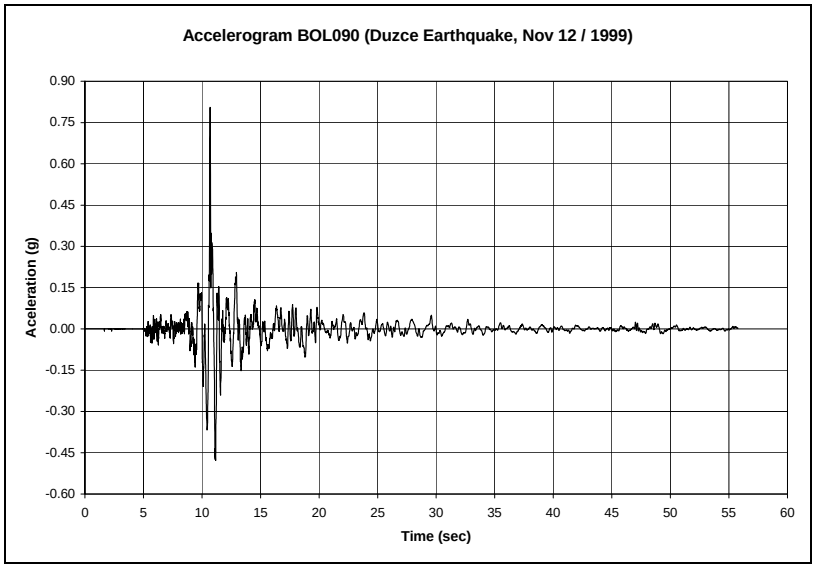

Figure A-13 Accelerations Recorded in Bolu (090 Component)

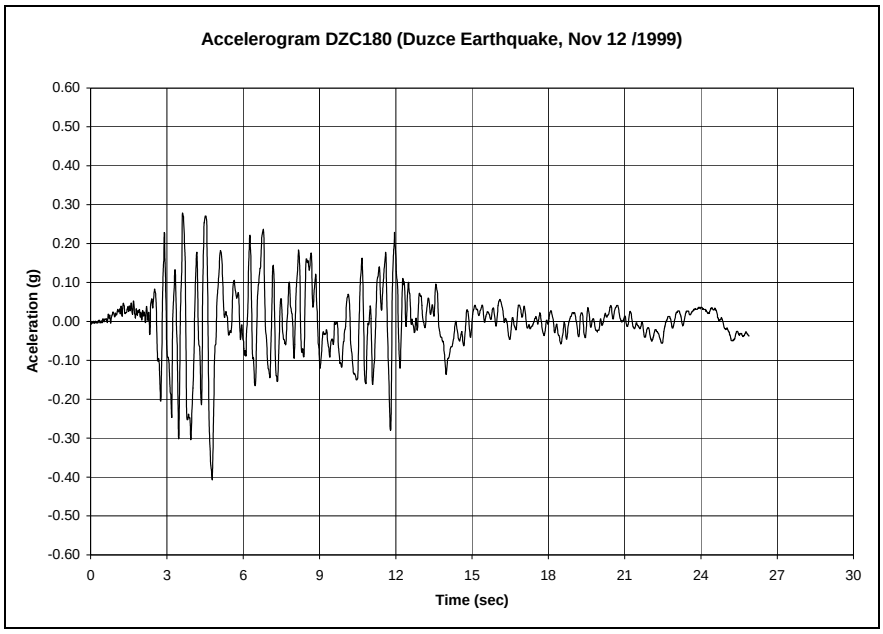

Figure A-14 Accelerations Recorded in Düzce (180 Component)

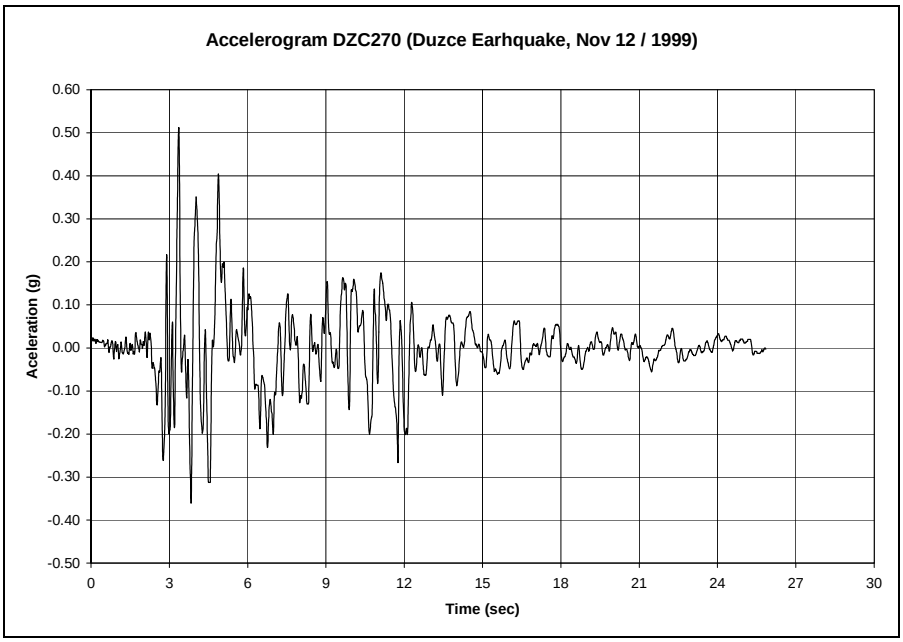

Figure A-15 Accelerations Recorded in Düzce (270 Component)

Appendix B

B.1 ELASTIC ACCELERATION RESPONSE SPECTRA FROM KOCAELI EARTHQUAKE

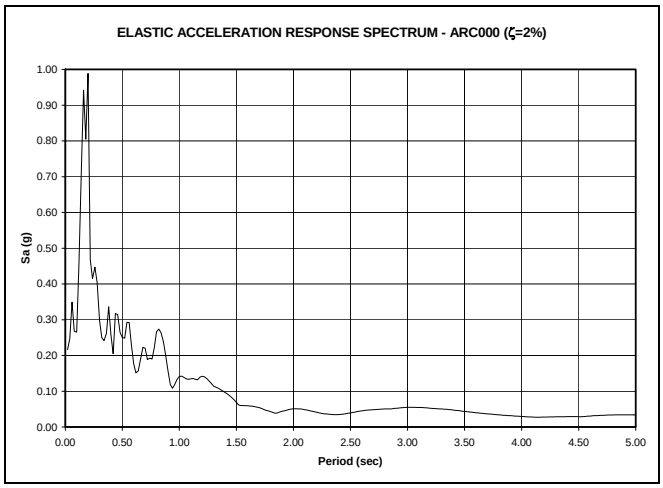

Figure B-1 Acceleration Response Spectrum for Ground Motion in Arcelik (000 Component)

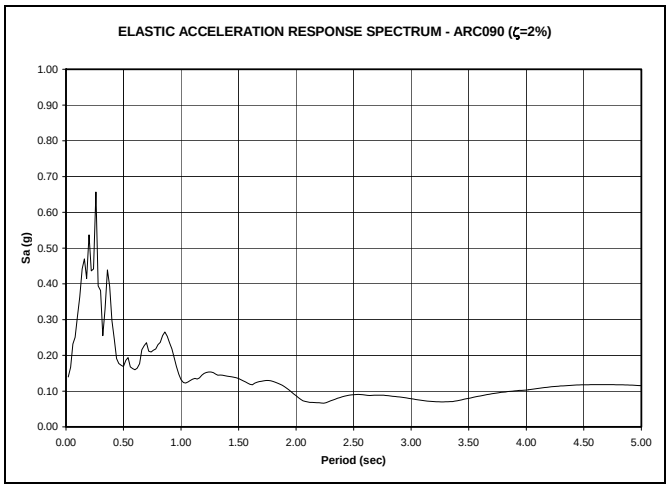

Figure B-2 Acceleration Response Spectrum for Ground Motion in Arcelik (090 Component)

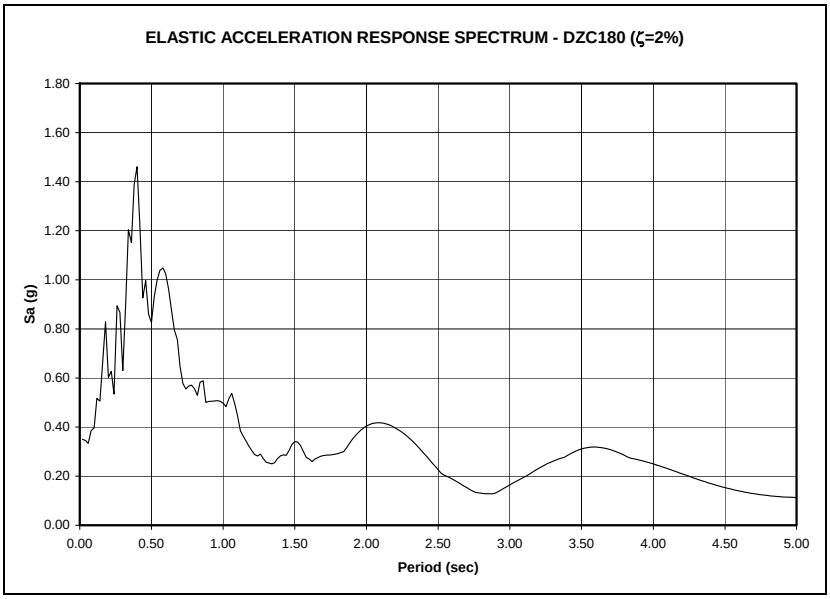

Figure B-3 Acceleration Response Spectrum for Ground Motion in Düzce (180 Component)

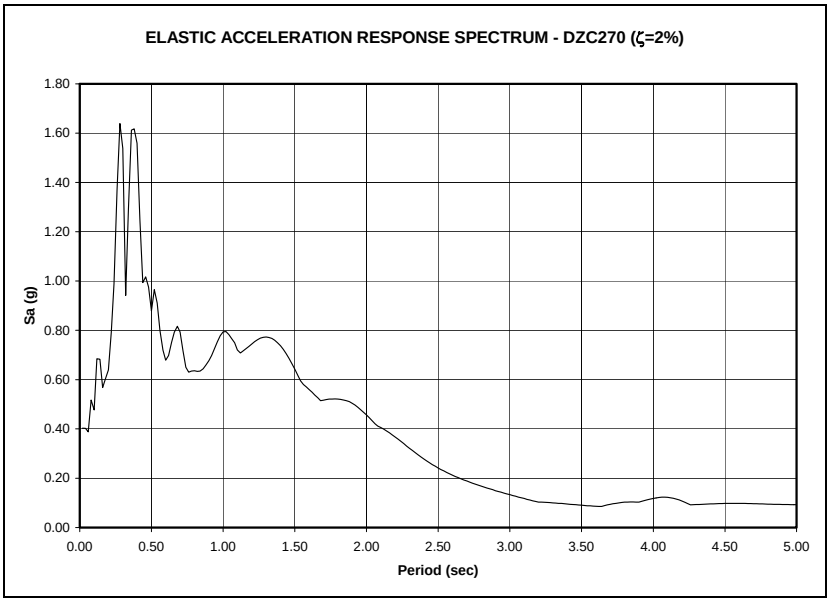

Figure B-4 Acceleration Response Spectrum for Ground Motion in Düzce (270 Component)

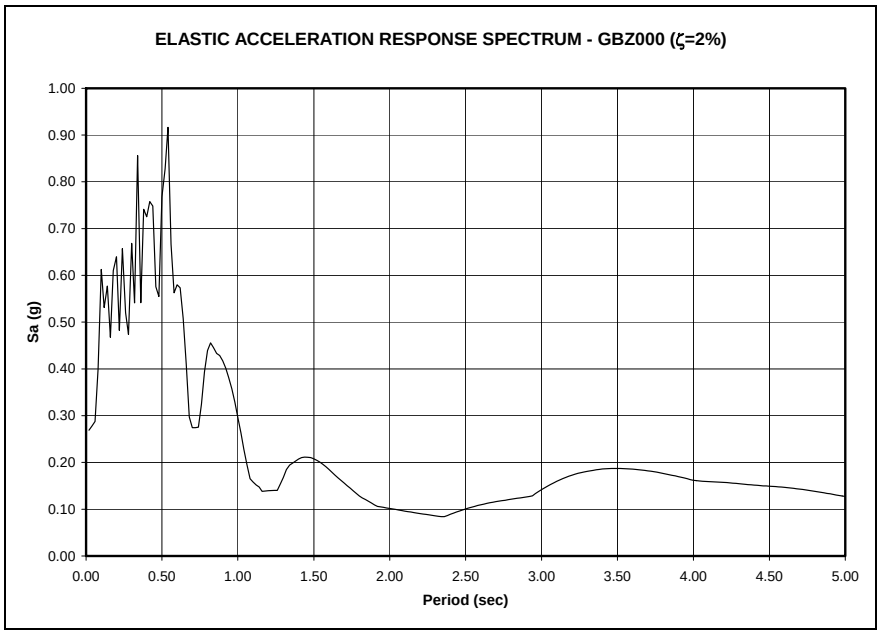

Figure B-5 Acceleration Response Spectrum for Ground Motion in Gebze (000 Component)

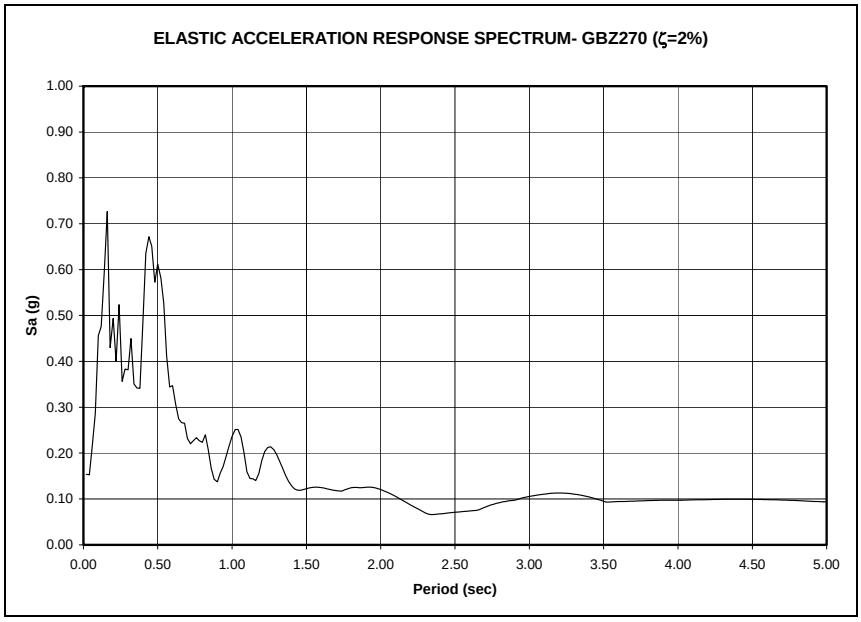

Figure B-6 Acceleration Response Spectrum for Ground Motion in Gebze (270 Component)

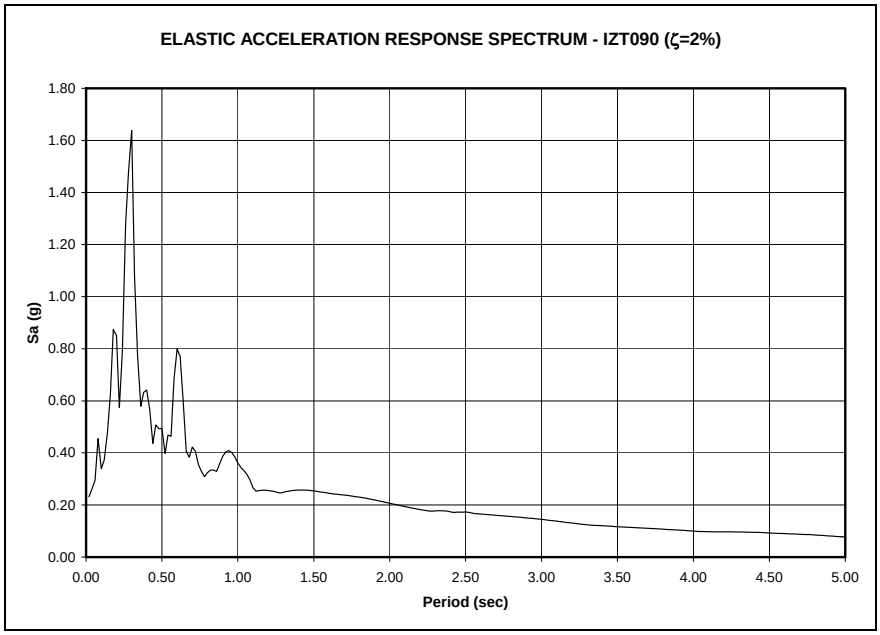

Figure B-7 Acceleration Response Spectrum for Ground Motion in Izmit (090 Component)

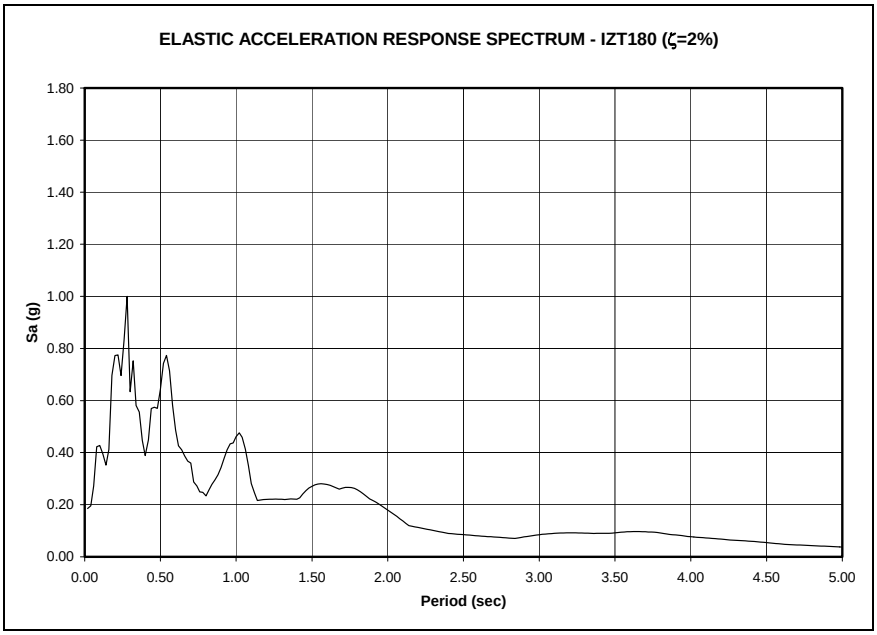

Figure B-8 Acceleration Response Spectrum for Ground Motion in Izmit (180 Component)

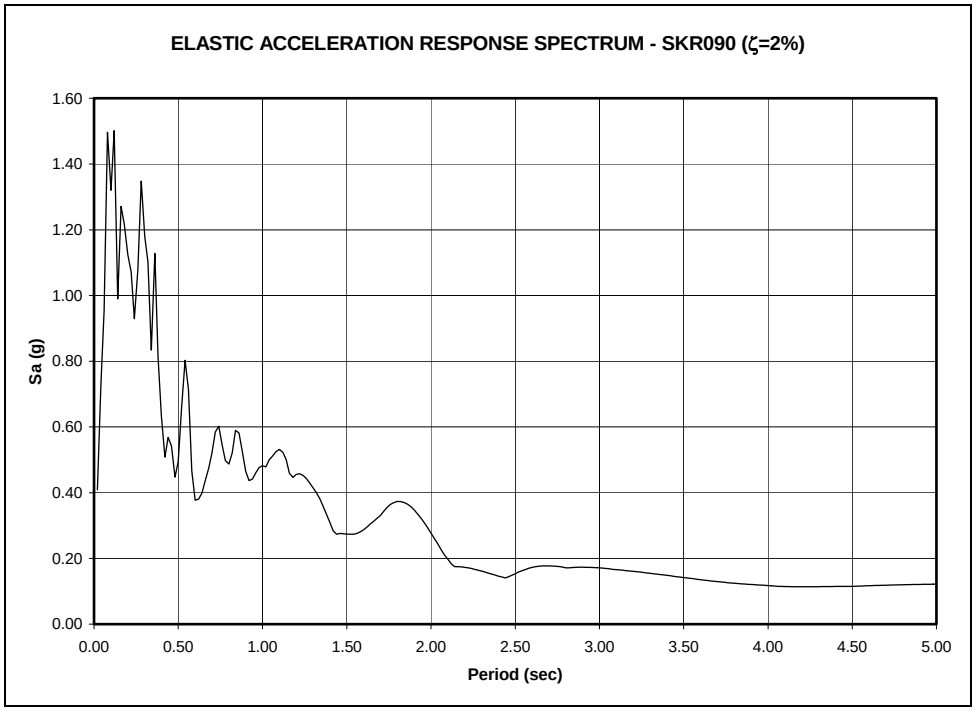

Figure B-9 Acceleration Response Spectrum for Ground Motion in Sakarya (090 Component)

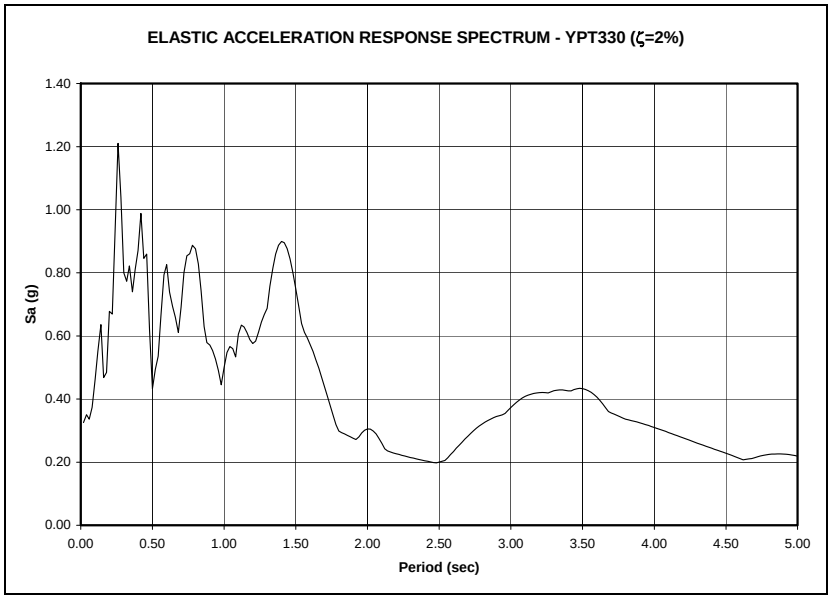

Figure B-10 Acceleration Response Spectrum for Ground Motion in Yarimca (330 Component)

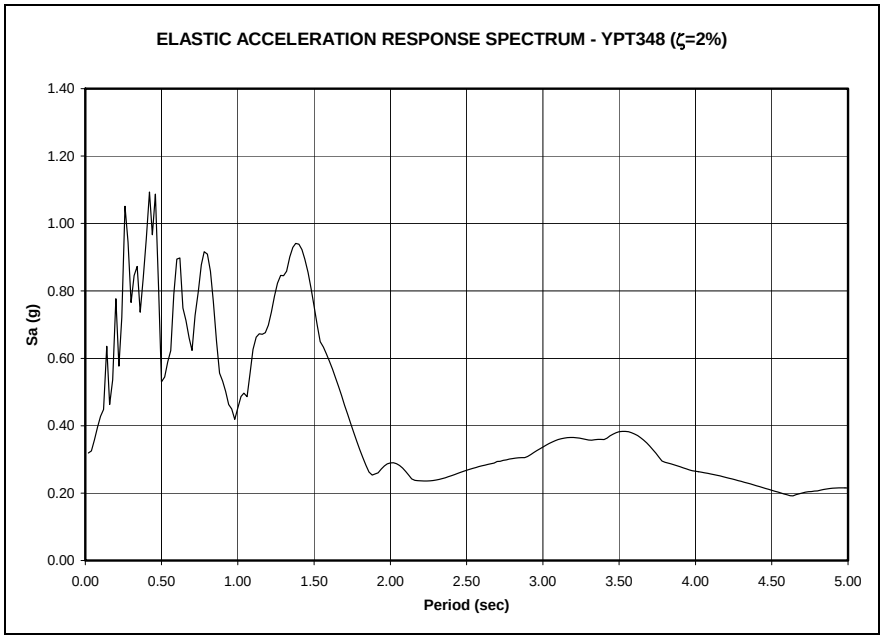

Figure B-11 Acceleration Response Spectrum for Ground Motion in Yarimca (348 Component)

B.2 ELASTIC ACCELERATION RESPONSE SPECTRA FROM DÜZCE EARTHQUAKE

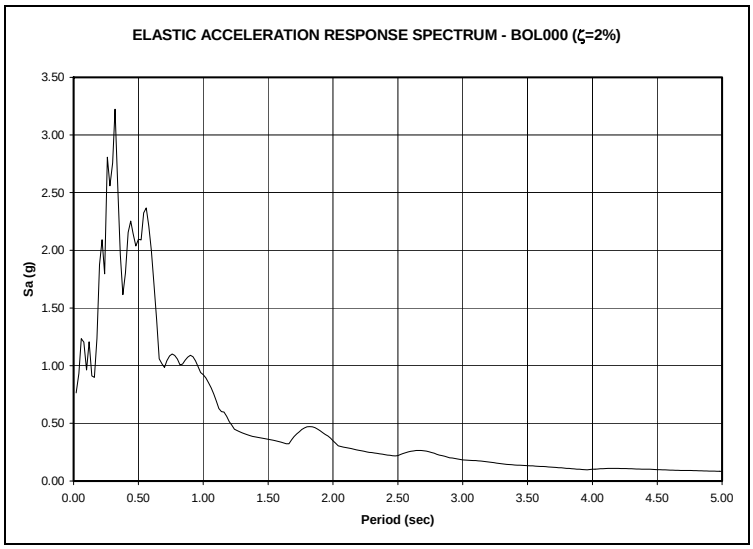

Figure B-12 Acceleration Response Spectrum for Ground Motion in Bolu (000 Component)

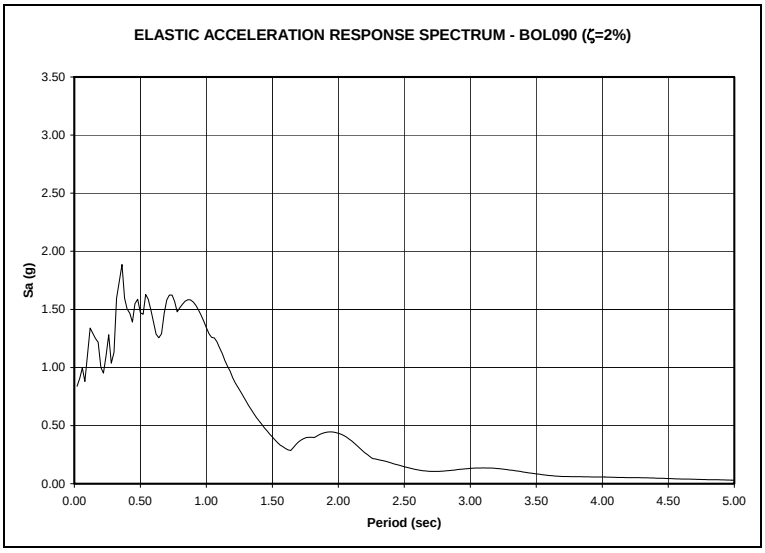

Figure B-13 Acceleration Response Spectrum for Ground Motion in Bolu (090 Component)

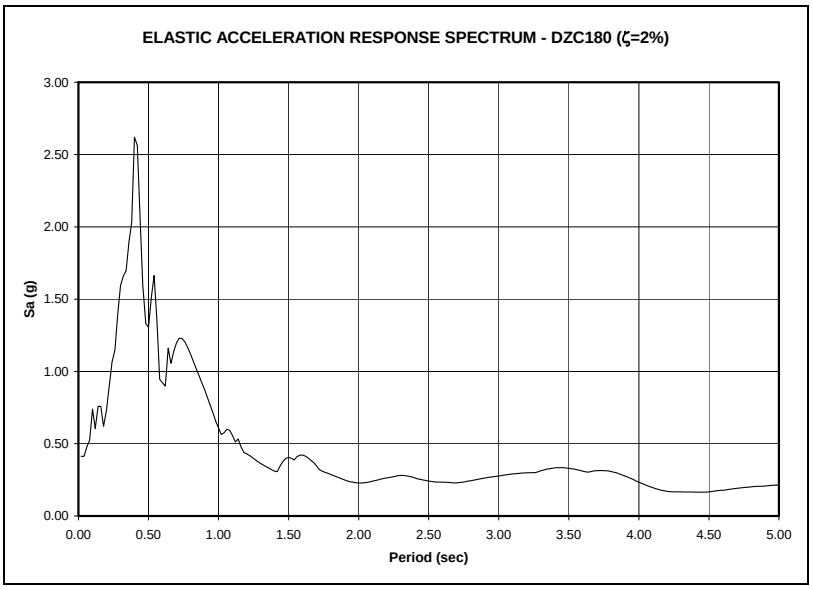

Figure B-14 Acceleration Response Spectrum for Ground Motion in Düzce (180 Component)

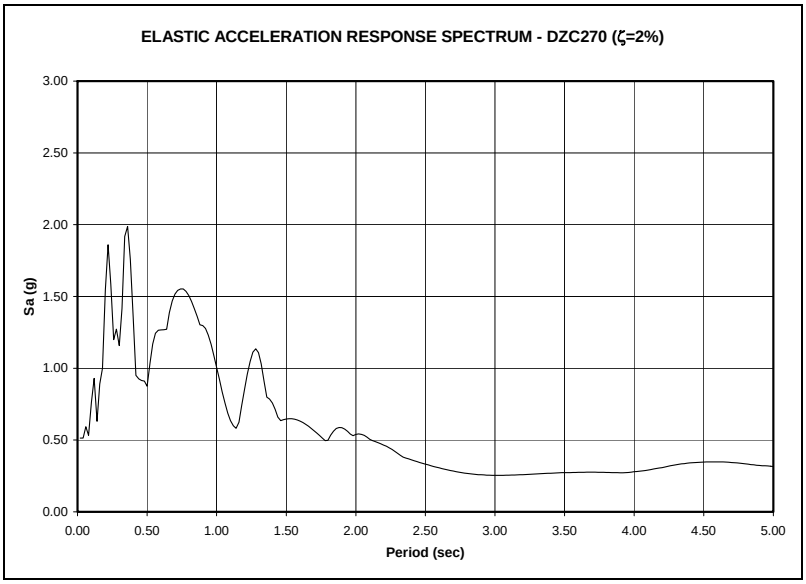

Figure B-15 Acceleration Response Spectrum for Ground Motion in Düzce (270 Component)

Appendix C

C.1 Calculated moment-curvature response for columns with 1% longitudinal reinforcement

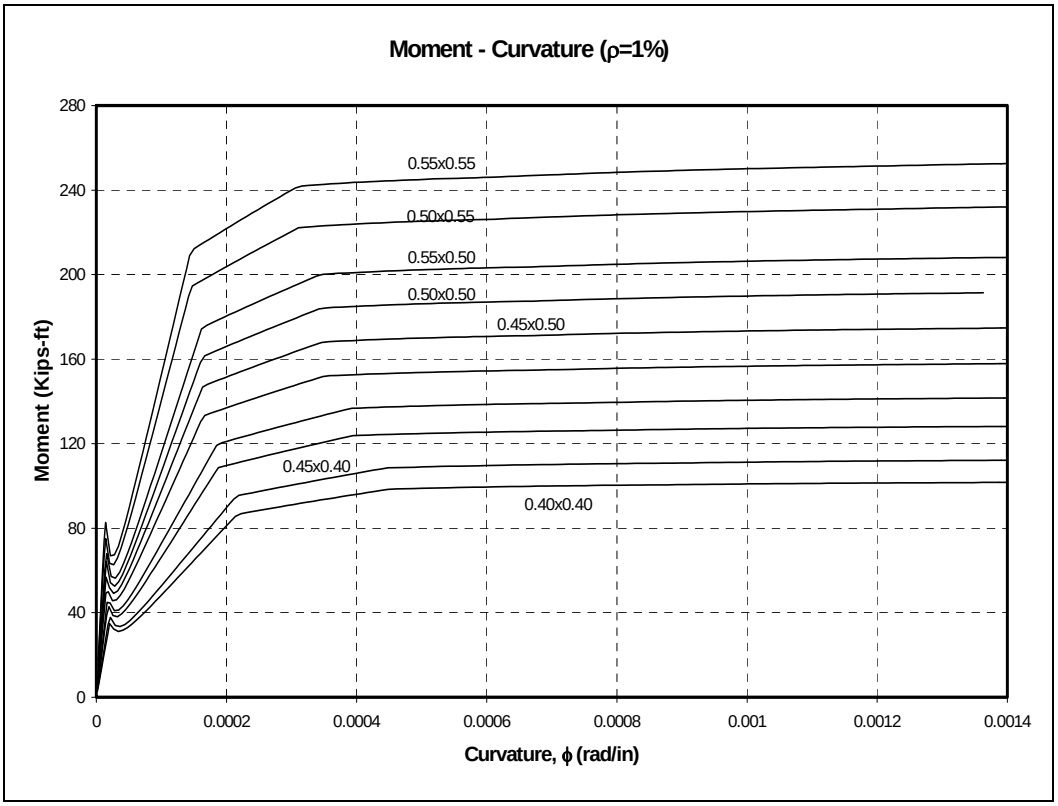

Figure C-1 Moment – Curvature Response for Small Columns with 1% Longitudinal Reinforcement

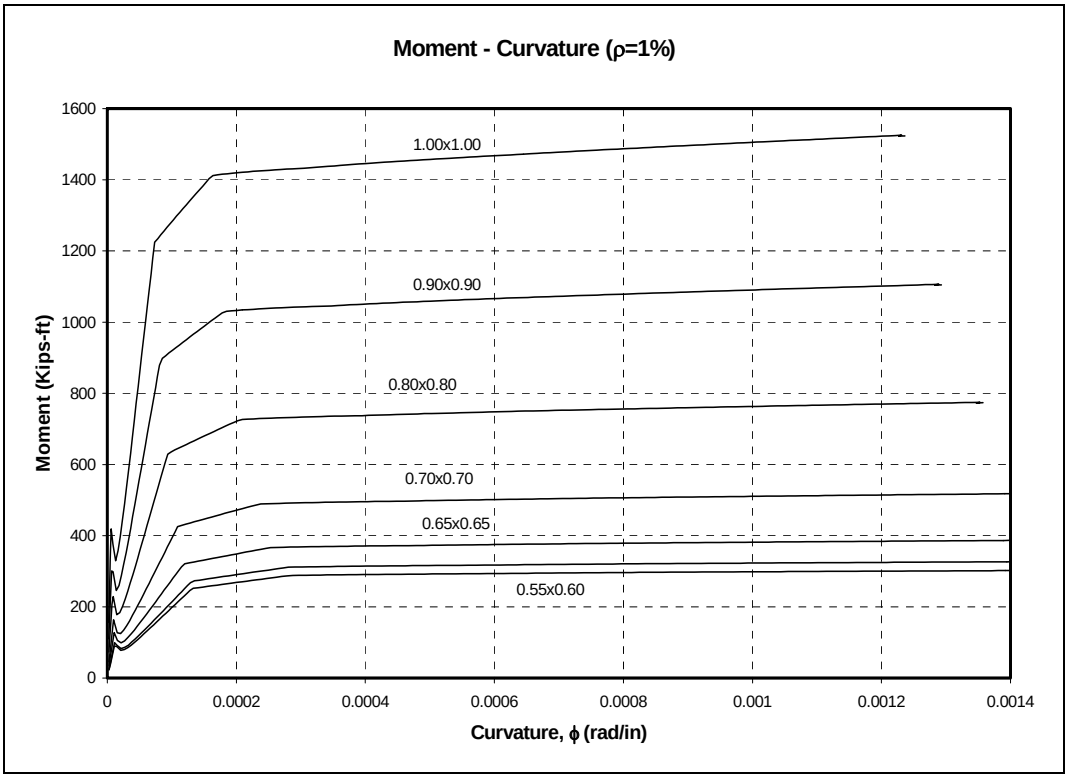

Figure C-2 Moment – Curvature Response for Large Columns with 1% Longitudinal Reinforcement

C.2 CALCULATED MOMENT-CURVATURE RESPONSE FOR COLUMNS WITH 2% LONGITUDINAL REINFORCEMENT

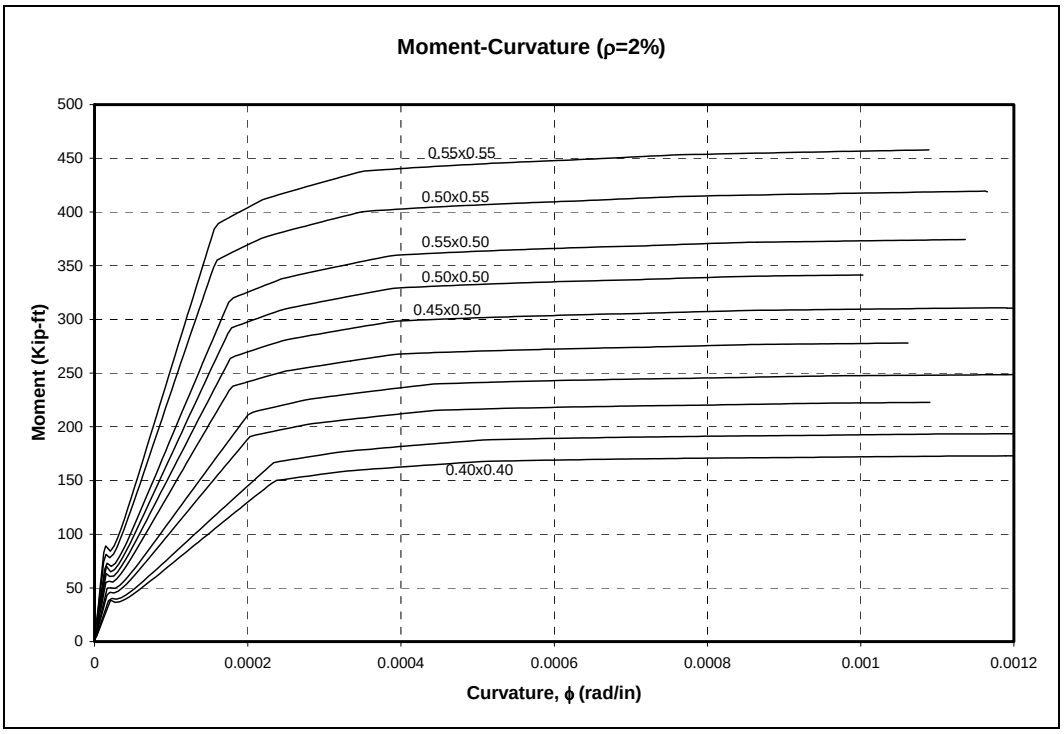

Figure C-3 Moment – Curvature Response for Small Columns with 2% Longitudinal Reinforcement

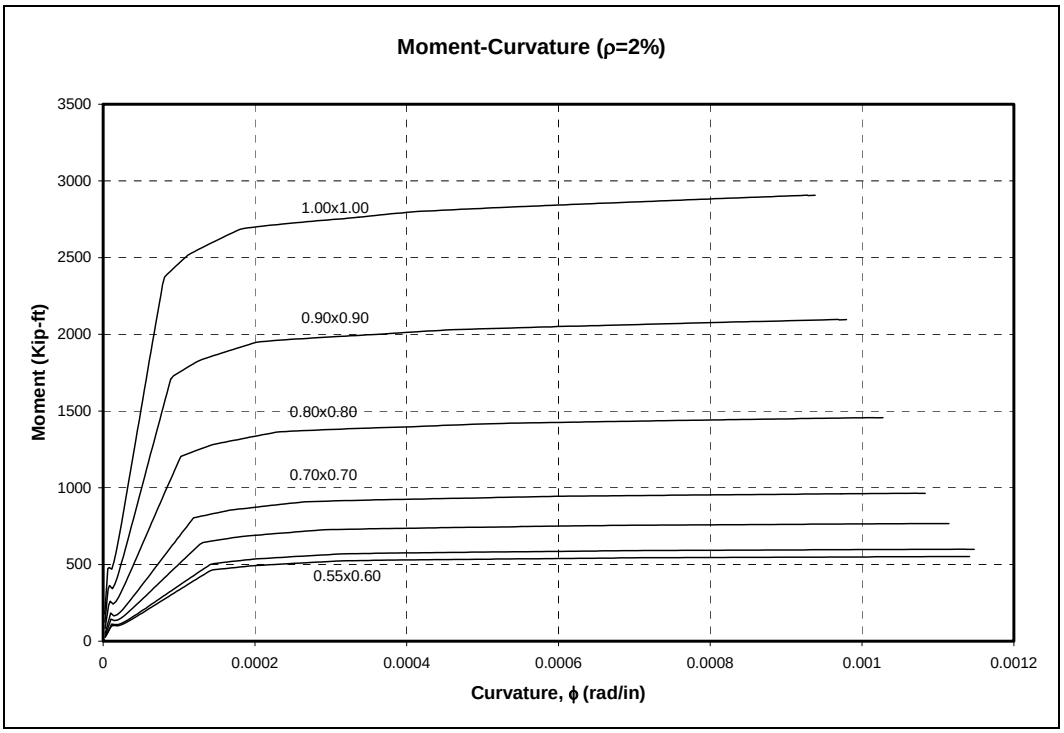

Figure C-4 Moment – Curvature Response for Large Columns with 2% Longitudinal Reinforcement

C.3 CALCULATED MOMENT-CURVATURE RESPONSE FOR COLUMNS WITH 3% LONGITUDINAL REINFORCEMENT

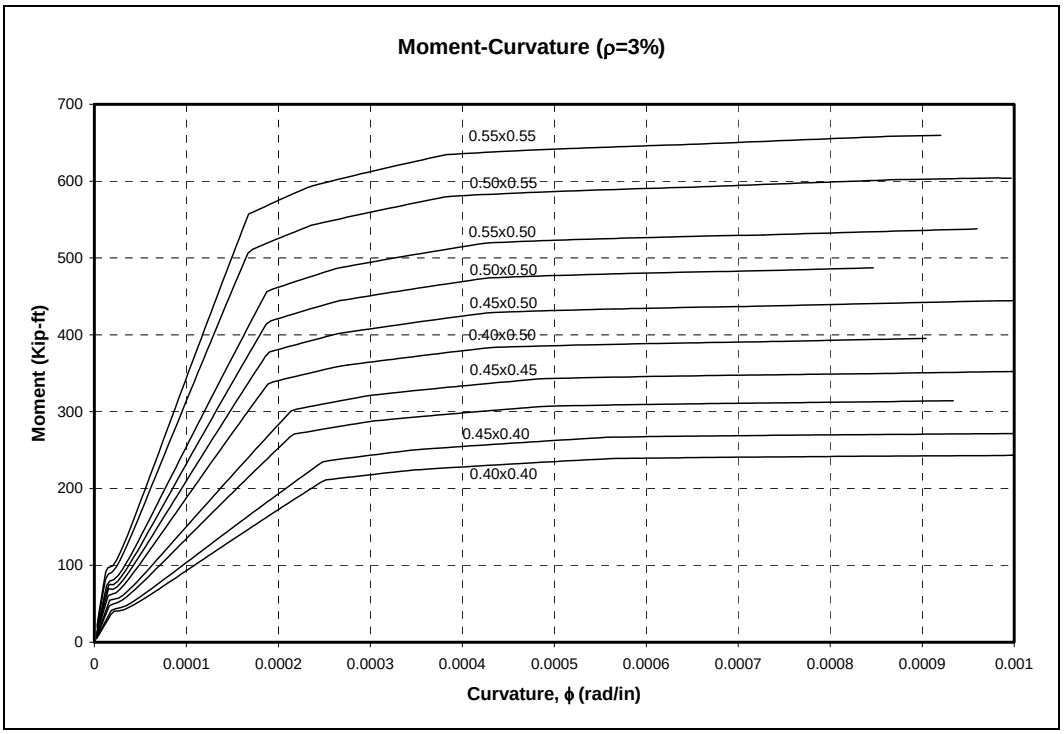

Figure C-5 Moment – Curvature Response for Small Columns with 3% Longitudinal Reinforcement

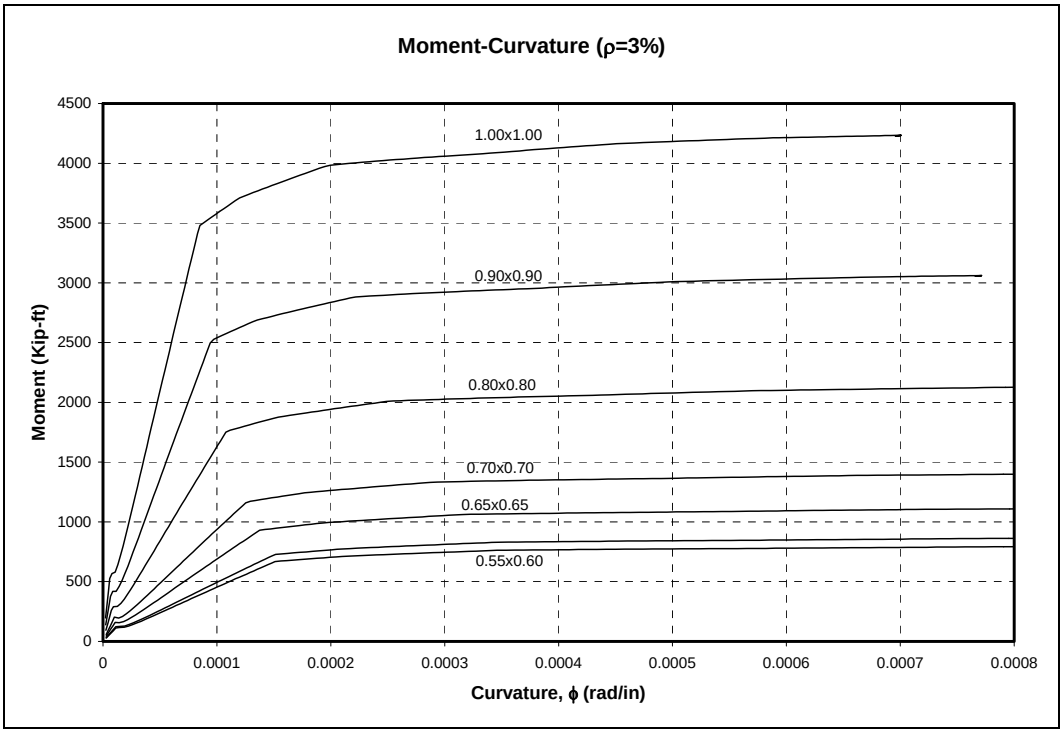

Figure C-6 Moment – Curvature Response for Large Columns with 3% Longitudinal Reinforcement

References

ACI 318-99 / ACI 318R-99 (1999) *Building Code and Commentary*. ACI Committee 318.

Anderson, J. G. (Coordinator) (2000). 1999 Kocaeli, Turkey, Earthquake Reconnaissance Report, Chapter 6. Implications for Seismic Hazard Analysis. *Earthquake Spectra* 16 (Supplement A): 113-137. December 2000. Earthquake Engineering Research Institute.

Aschheim, M. (Coordinator) (2000). 1999 Kocaeli, Turkey, Earthquake Reconnaissance Report, Chapter 11. Performance of Buildings. *Earthquake Spectra* 16 (Supplement A): 237-279. December 2000. Earthquake Engineering Research Institute.

Atakoy, H. (1999). *17 August Marmara Earthquakes and the Precast Concrete Structures Built by TPCA Members*. Turkish Precast Association. Ankara, Turkey. 12p.

Garcia, Luis E. (2000) *RespSpect2000 ver1.2*®. Bogotá, Colombia.

Hognestad, E. (1951). A Study of Combined Bending and Axial Load in Reinforced Concrete Members. Bulletin 399, University of Illinois Engineering Experimental Station, Urbana, IL. November 1951. 128p.

Johnson, G. (Coordinator) (2000). 1999 Kocaeli, Turkey, Earthquake Reconnaissance Report, Chapter 14. Industrial Facilities. *Earthquake Spectra* 16 (Supplement A): 311-350. December 2000. Earthquake Engineering Research Institute.

Karaesmen, E. (2001). *Prefabrication in Turkey, Facts and Figures*. June 2001. Middle East Technological University, METU. 28p.

Lettis, W. (Coordinator) (2000). 1999 Kocaeli, Turkey, Earthquake Reconnaissance Report, Chapter 1. Geology and Seismicity. *Earthquake Spectra* 16 (Supplement A): 1-9. December 2000. Earthquake Engineering Research Institute.

Moehle, J. P. (1992). Displacement-Based Design of RC Structures Subjected to Earthquakes. *Earthquake Spectra* 8 (3): 403-428. 1992. Earthquake Engineering Research Institute.

Rathje, E. (Coordinator) (2000). 1999 Kocaeli, Turkey, Earthquake Reconnaissance Report, Chapter 4. Strong Ground Motions and Site Effects. *Earthquake Spectra* 16 (Supplement A): 65-96. December 2000. Earthquake Engineering Research Institute.

Scawthorn, C. and G. S. Johnson. (2000). *Preliminary Report Kocaeli (Izmit) Earthquake of 17 August 1999*. Engineering Structures 22: 727-745.

Shimazaki, K. and M.A. Sozen (1984). *Seismic Drift of Reinforced Concrete Structures*. Research Reports, Hazama-Gumi, Ltd., Tokyo, Japan, 145-166.

Turkish Precast Concrete Association. On-line. Available URL: http://www.prefab.org.tr